Energy Savings in Air Handling Unit by Using Heat Pipe Heat Exchanger

Saw Yu Mon [(1)], Ei Thandar Myo [(2)]
[(1)] Mandalay Technological University, Myanmar
[(2)] Mandalay Technological University, Myanmar

Email: sawyumon.82@gmail.com

ABSTRACT: In this paper, the theoretical analysis of heat pipe heat exchanger in air handling unit concerning with energy saving factors. The main purpose of this paper is to study the possible energy saving with various face velocities of applying wraparound heat pipe heat exchanger in air handling unit of central air conditioning system. According to theoretical results, the inlet air temperature of 313K drops to 304.4K after passing through the precool section and provides the supply conditions of 293.27K and 54% which meet the comfort requirements at 1.32m/s and the higher face velocity will lead the above results into the opposition manner. The energy consumption that can be saved from this design is 14.1kW of precool and 14.7 kW of reheat actions across the heat exchanger with temperature effectiveness of 30.87%. In addition to that, it can also provide higher energy savings and temperature effectiveness.

KEYWORDS*: wraparound, energy saving, effectiveness, face velocity, precool, reheat*

1. INTRODUCTION

Heat pipe heat exchangers (HPHX) are energy efficient devices using the excellent thermal transfer properties of heat pipe for heat recovery application in air conditioning system. And heat pipe heat exchangers become the trending energy efficiency devices. They can provide sensible cooling by pre-treating the incoming air before passing through the active cooling coil (chilled water or direct expansion (DX)) and also provide the passive reheating action freely to supply air.

The other advantage of HPHX is that it can reduce the cooling demand of cooling coil, in the other way, it can reduce the chiller size by providing precooling action and helps the cooling coil to use it more capacity to extract excess moisture called enhancing dehumidification. Wraparound heat pipe heat exchanger (WAHPHX) can be considered as the most appropriate device to provide energy efficiency advantages to these situations because it can improve the performance of the cooling coil with the aids of precooling and reheating sections.

It consists of precool coil and reheat coil wrapping around the cooling coil. The heat from the incoming air is picked up in the evaporator section which is called sensible cooling and reduces the demand loads of the cooling coil. Moreover, the discharged cooler air is reheated again from the free passive heat recovery at the condenser section for comfort environment. Wraparound heat pipe heat exchanger in air handling unit are shown in Fig. 1.

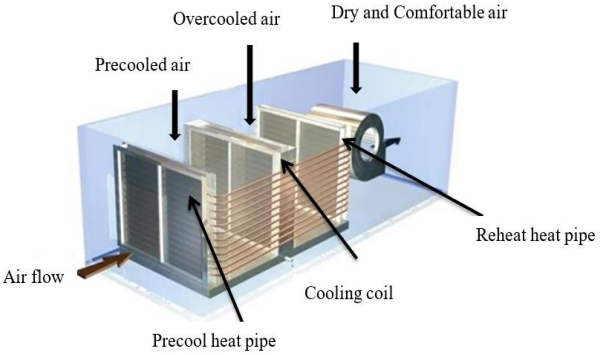

Fig 1. Wraparound Heat Pipe Heat Exchanger in Air Handling Unit [11]

Air conditioning provides the comfort environment by maintaining it in the recommended temperature and relative humidity. In conventional air conditioning system, the incoming air is cooled down below its dew point temperature at the active cooling coil of the chiller. As a result, the cooling demand is high for the cooling coil to lower the high ambient temperature to its dew point and at the same time, the additional heating system is required to reheat the freezing air leaving the coil before delivering to the space.

Heat pipe heat exchangers (HPHX) become the trending efficient devices to solve these problems. They are used to precool the incoming air to reduce the load for the cooling coil and more able to apply efforts on moisture removal. In addition to that, it also provides free passive reheating which is obtained from the discharged heat in the condenser section.

2. DESIGN THEORY OF HEAT PIPE HEAT EXCHANGER

Most of the specification data are taken from the air handling unit (AHU) from PULLMAN Hotel, Mandalay. The length of the evaporator (precool) and condenser (reheat) sections are taken from the internal width dimension of AHU unit, but the adiabatic length is determined by considering the position of wraparound heat pipe heat exchanger with the cooling coil. The important thing which must be taken into consideration is the distance between the cooling coil

and the reheat section. The distance between them has to be at least 6 inches or greater in order to avoid the moisture transferring to the reheat coil while the precool section can be located close to the cooling coil. The heat pipe with the driven capillary force in the wick structure to operate working fluid is known as wicked heat pipe and wick structure materials is copper and type is sintered. The complete specifications of heat pipe heat exchanger are listed in the following Table 1.

Table 1. Specifications of Heat Pipe Heat Exchanger

Sr.	Parameter	Symbols	Value	Unit
1.	Face velocity	v	1.32	m/s
2.	Inlet air temperature of heat pipe heat exchanger	T_1	313	K
3.	Inlet air relative humidity	$\emptyset_1$	55	%
4.	Longitudinal pitch	S_L	21.43	mm
5.	Transverse pitch	S_T	31.75	mm
6.	Number of tubes in row (transverse)	N_T	23	-
7.	Number of tubes in row (longitudinal)	N_L	12	-
8.	Heat transfer length	L	1.35	m
9.	Density of Wick structure material (copper)	ρ	8940	kg/m^3

The tubes of wraparound heat pipe are arranged individually in a staggered arrangement position.

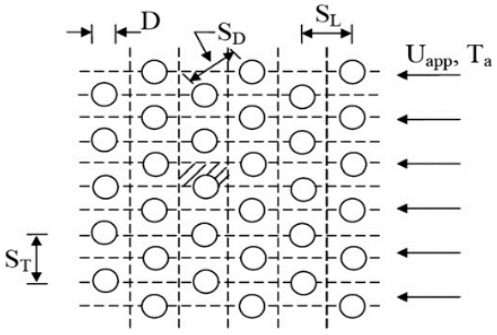

Fig 2. Schematic Diagram of Tubes of Heat Exchanger in Staggered Arrangement

The arrangement of the tubes in the tube bank is described by the transverse pitch S_T, longitudinal pitch S_L, and the diagonal pitch S_D between tube centers. Fig.2 shows schematic diagram of tubes of heat exchanger in staggered arrangement.

(i) Maximum Velocity of Air

The maximum velocity occurs at the minimum flow area between the tubes,

$$v_{max} = \frac{S_T}{S_T - D} \times v \qquad (1)$$

where,

v_{max} - maximum velocity of the air (m/s)

S_T - transverse pitch (m)

D - diameter of the tube (m)

v - velocity of the air (m/s)

(ii) Reynolds Number, $Re_D = \frac{\rho \times v_{max} \times D}{\mu}$

(2)

(iii) Nusselt Number

$$Nu_D = 0.35(S_T/S_L)^{0.2} Re_D^{0.6} Pr^{0.36} (Pr/Pr_s)^{0.25}$$

(3)

Average Nusselt Number,

$$Nu_{D_{NL}} = F \times Nu_D$$

(iv) Heat Transfer Coefficient

$$h = \frac{Nu_{DNL} \times k}{D} \qquad (4)$$

where,

h - heat transfer coefficient (W/m^2K)

Nu_{DNL} - average Nusselt number

K - thermal conductivity of air (W/mK)

The heat transfer surface area is the contact surface area of the tube pass through the air,

$$A_S = N \times \pi \times D \times L$$

(v) Total Number of Tubes

$$N = N_T \times N_L$$

(5)

(vi) Mass Flow Rate of Air

$$\dot{m_a} = \rho \times v \times N_T \times S_T \times L$$

(6)

where,

$\dot{m_a}$ - mass flow rate of air, (kg/s)

ρ - density of air (kg/m^3)

v - velocity of air (m/s)

N - number of tubes in transverse surface

S_T - transverse pitch (m)

L - length of the copper tube (m)

(vii) Outlet Temperature of Precool and Reheat Sections

$$T_e = T_s - (T_s - T_i)\exp(\frac{-A_s h}{\dot{m} C_p})$$

(7)

where,

T_e- air exit temperature after precool section T_2 (°C)

T_e- air exit temperature after reheat section T_4 (℃)

T_s-surface temperature of precool and reheat sections (℃)

T_i - inlet temperature at precool section T_1 (℃)

T_i - inlet temperature at reheat section (or) exit temperature after active cooling coil T_3 (℃)

(viii) Effectiveness of Wraparound Heat Pipe Heat Exchanger (WAHPHX)

The effectiveness of WAHPHX is the ratio of the actual amount of transferred by the heat exchanger relative to the maximum heat that could be transferred.

The sensible effectiveness, ε is given by,

$$\varepsilon = \frac{T_4 - T_3}{T_1 - T_3} \quad (8)$$

(ix) Estimated Energy Savings

Wraparound heat pipe heat exchanger saves energy by reducing the cooling demands of the cooling coil and improving the performance of it. It reduces the temperature of the incoming air which provides precool saving by reducing the load of the cooling coil.

Energy savings (kW),

$Q = 1.1\ CFM\ (\Delta T) \times 1/3412.14$ (9)

where,

CFM - air flow rate (ft^3/min)

ΔT - temperature drop after precool coil or reheat coil (°F)

- $T_4 - T_3$ for reheat savings
- $T_1 - T_2$ for precool savings

3. RESULTS OF HEAT PIPE HEAT EXCHANGER DESIGN

The tubes of the wraparound heat pipe are arranged as staggered position in the direction of the fluid flow. The tube bank of heat pipes is positioned around the cooling coil and it is divided into two sections called precool and reheat.

Table 2. Results data for Required Flow Properties

Sr	Parameter	Results Value
1.	Maximum velocity of air, V_{max}	2.84 m/s
2.	Reynolds number, Re_D	2845.0206
3.	Nusselt number ,Nu_D	37.94
4.	Average Nusselt number, Nu_{DNL}	37.45
5.	Heat transfer coefficient, h	58.55 W/m^2K
6.	Total number of tube, N	276
7.	Mass flow rate of air,m_a°	1.467 kg/s

The main parameter that will be calculated from this design is the exit temperatures of these two sections. The corresponding effectiveness and energy savings are calculated from the value of these exit temperatures by changing the rows of heat pipe and velocity. Results data for required flow properties are shown in Table 2.

At the design condition of face velocity 1.32 m/s, the appropriate rows of heat pipe which can provide the values that meet the comfort conditions is turned out as 12 rows. The surface temperature of tubes in evaporator section and condenser section of heat pipe heat exchanger are different depending on the various velocities. The following Table 3 provides the surface temperatures of tubes obtained by taking the average value of respective values of different rows of heat pipe.

Table 3. Surface Temperature of Tubes in Evaporator and Condenser Sections at Different Velocities

Face Velocity (m/s)	Evaporator Surface Temperature (K)	Condenser Surface Temperature (K)
1.32	297.22	300.95
2	300.944	296.956
3	304	294.766

The outlet temperature of evaporator section of heat pipe heat exchanger is obtained,

$$T_e = T_s - (T_s - T_i)\exp\left(\frac{-A_s h}{\dot{m} C_p}\right)$$

T_2= 304.39 K

For condenser outlet temperature, the inlet temperature of the section is the coil outlet temperature and the result is obtained as,

T_4 =293.47 K

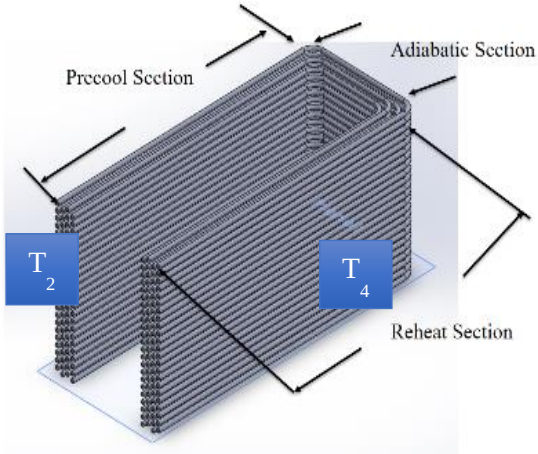

Fig 3. Rows of Wraparound Heat Pipe Heat Exchanger

Rows of hear pipe heat exchanger are expressed in Fig.3. The theoretical values of temperature and relative humidity at each stage for central air conditioning system with heat pipe heat exchanger with varied velocities are shown in Fig.4 and Fig.5. In these figures T_2 refers to temperature leaving precool section, T_4 refers to temperature leaving reheat section, $\emptyset_2$ refers to relative humidity after precool section and $\emptyset_4$ refers to relative humidity after reheat section.

In Fig.4, the obtained leaving reheat section temperature drop is inversely proportional to the increasing value of face velocity. Then the leaving precool section temperature drop is directly to the face velocity growing. At the design condition of velocity 1.32 m/s, the outlet temperature of the precool section is resulted as 304.4K and reheat section (supply conditions) is 293.47K at inlet air temperature of heat pipe heat exchanger is 313K.

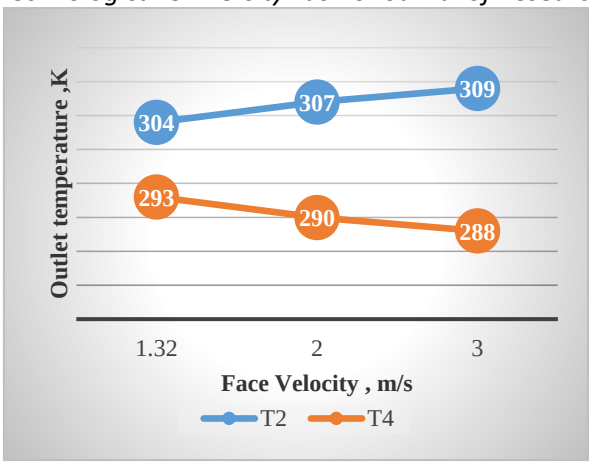

Fig 4. Results of Outlet Temperature with Varies Face Velocity

Relative humidity (RH) with various face velocity are shown in Fig.5. In this figure, precool section outlet RH value is 88% and supply condition RH value is 54% at design velocity 1.32m/s.

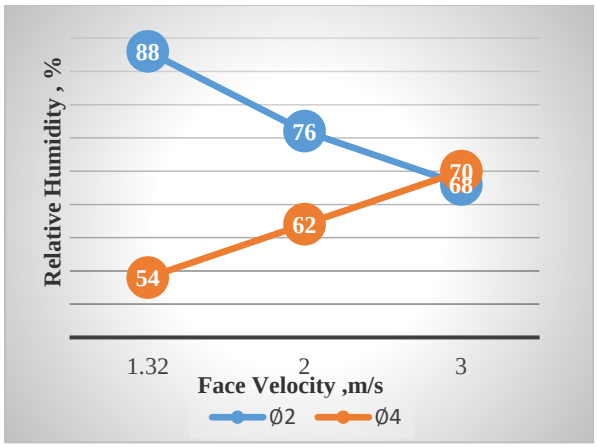

Fig 5. Results of Relative Humidity with Varies Face Velocity

The ideal range for indoor humidity during summer time is about 30% - 50%. Therefore, supply condition 54%RH is comfortable value at design face velocity. As a results, air condition at precool section is 304K & 88% RH and reheat section (supply condition) is 293K & 54%RH.

Table 4. Results data for Energy Saving at Various Face Velocity

Sr.	Parameter	Face velocity, v(m/s)		
		1.32	2	3
1	Precool savings, $Q_{precool}$, (kW)	14.1	9.62	6.39
2	Reheat savings, Q_{reheat} (kW)	14.7	9.95	7.21
3	Effectiveness , ε (%)	30.87	21.3	15.4

Table 4 shows in results data for energy saving in heat pipe heat exchanger at various face velocity. From the results described in tables the energy savings with conversely proportion to the face velocity. According to the comfort living limitations, the most suitable solution is 12 rows wraparound heat exchanger which provides precool savings of 14.1kW and reheat savings of 14.7 kW at designed velocity. In the same way with energy saving factors, the effectiveness of wraparound heat exchanger increases and decreases with the face velocity. And it provides the effectiveness of 30.87% at the design condition which is obtained from the 12 rows wraparound heat exchanger.

4. DISCUSSIONS AND CONCLUSIONS

The design and air conditioning system of wraparound heat pipe heat exchanger is performed in this paper. In this analysis, the staggered tube arrangement of heat pipe heat exchanger design is conducted. According to theoretical results, the results are obtained as 276 of total number of heat pipe and it can supply 293.47K and 54% at the design condition of 1.32m/s with the inlet temperature of 313K. And it also provides precool savings, $Q_{precool}$ of 14.1kW and reheat savings, Q_{reheat} of 14.7kW with effectiveness of 30.87%. By increasing face velocity 1.32m/s to 2m/s and 3m/s, energy saving condition is become lesser than design velocity. Therefore, it can be concluded that the application of wraparound heat pipe heat exchanger in air handling unit is applicable for saving energy consumption. The air conditioning system with wraparound heat pipe heat exchanger can save the energy consumption by reducing the load of cooling coil and provide the free reheat actions passively.

ACKNOWLEDGEMENTS

The first of all, the author wish to express my deep gratitude to Dr. Ei Ei Htwe, Acting Rector, Mandalay Technological University, for her kindness valuable permission to summit this paper.

The author also grateful to Dr. Win Pa Pa Myo, Professor and Head, Mechanical Engineering Department, Mandalay Technological University, for her helpful, invaluable suggestions and comments during the submit this paper.

Moreover, special thanks to my partner, Ma Ei thandar Myo for her kind suggestions the entire process of this research work. This paper would not have been possible without her support. Finally, the author would like to say thank to her family especially her parents for their noble support, encouragement, and guidance throughout her entire life.

REFERENCES

[1] Tushar, S. J. and Mandar, M. L.: A case study on energy savings in air conditioning System by heat recovery using heat pipe heat Exchanger, (2016).

[2] Ong, K. S.: Review of heat pipe heat exchangers for enhanced dehumidification and cooling in air conditioning systems, (2014).

[3] Gode, S.D., Tushar, S. J. and Lele, M.M.: Operating limits of heat pipe heat exchanger for air conditioning application, (2015).
[4] Tushar, S. J. and Mandar, M. L.: Theoretical Energy Saving Analysis of Air Conditioning System Using Heat Pipe Heat Exchanger for Indian Climate Zones, (2015).
[5] Faghri, A.: Heat Pipes Review, Opportunities and Challenges, Department of Mechanical Engineering, University of Connecticut, Storrs, CT 06269, U.S.A., Global Digital Central, (2014).
[6] Ong.K.S.: Experimental performance of R-134a-Filled and Water-Filled Loop Heat Pipe Heat Exchanger, (2010).
[7] Gode, S.D., Tushar, S. J. and Lele, M.M.: Operating limits of heat pipe heat exchanger for air conditioning application, (2015).
[8] Tushar, S. J. and Mandar, M. L.: Theoretical Energy Saving Analysis of Air Conditioning System Using Heat Pipe Heat Exchanger for Indian Climate Zones, (2015).
[9] Faghri, A.: Heat Pipes Review, Opportunities and Challenges, Department of Mechanical Engineering, University of Connecticut, Storrs, CT 06269, U.S.A., Global Digital Central, (2014).
[10] Ahmadzadehtalatapeh, M. and Yau, Y.H.: A review on the application of horizontal heat pipe heat exchanger in air conditioning systems in the tropics, (2009).
[11] https://www.spc-hvac.co.uk/

DESIGN OF CENTRIFUGAL COMPRESSOR IMPELLER FOR FERTILIZER PLANT

Aye Thida San(1), Soe Myat Thu(2), Khin Thandar Aung(3)
(1)Technological University (Pathein), Myanmar
(2), (3) Technological University (Mawlamyine), Myanmar

Email: ayethidasan1980@gmail.com

ABSTRACT*:* An impeller is the essential part of centrifugal compressor. The centrifugal compressor is a dynamic compressor depending on a rotating impeller to compress the air. This paper is mainly focus on design calculation of centrifugal compressor impeller for fertilizer plant. The main purpose of this work is to reduce the inlet and outlet diameter and width of impeller by changing the flow rate. The design calculation is considered based on the existing fertilizer plant. The engine flow rate 0.13m^3/s and the speed 38000 rpm will used to calculate the design of impeller. The necessary data are collected from fertilizer plant which is located in Pathein. The designed data are the inlet width is 0.008m, the outlet width is 0.003m, the hub diameter is 0.021m and the eye diameter is 0.042m. The number of blade is 13 and the efficiency is 95 percent. According to the calculated results, it is found that the diameter and width of the impeller are reduced and efficiency is improved.

KEYWORDS: *Centrifugal compressor, Impeller, Velocity, Efficiency*

1. INTRODUCTION

The centrifugal compressor consists essentially of a stationary casing containing a rotating impeller which imparts a high velocity to the air, and a number of fixed diverging passages in which the air is decelerated with a consequence rise in static pressure. Air is sucked into the impeller eye and whirled around at high speed by the vanes on the impeller disc. At any point in the flow of air through the impeller, the acceleration is obtained by a pressure head, so that the static pressure of the air increases from the eye to the tip of the impeller in HIH Saravanamuttoo, et al. (2013).

Centrifugal compressor has the potential for both lower pressure ratio and lower efficiency than the axial flow compressor. Construction, power plant, process industry, assembly plant, air conditioning and refrigeration are widely used in centrifugal compressors. Pumps, compressor and electric motor are the same for power conversion machines in Ronald P,et al. (1982). A small gas turbine is used in centrifugal compressor drive gas turbine compressor trains. Centrifugal compressor compresses gas by means of blades on a rotating impeller which transfers rotary motion to the gas. This increases the pressure. The advantages of a centrifugal compressor are long life and it can increase the enough of pressure for efficient combustion with only one stage. But initial costs are higher and air flow is difficult to change in ambient conditions according to H.K. Ludtke (2004). R.C. Reid, et al (1987) described that the air flow for a centrifugal compressor is much decrease than for an axial flow compressor and its pressure ratio is generally smaller. Hence, it uses in small engines.

Rama S.R. Gorla (2003) states that there are two types of centrifugal compressor are single stage and multi stage. The rotate of impeller with a high velocity and it connects the air is a high speed, due to which there is a low pressure rise during its radial flow in the impeller. The air is entering the diffuser where a substantial part of its kinetic energy is transferred into static pressure. Then, the air is entering the casing and the outlet pipe, where some more kinetic energy is transferred into pressure energy. In the centrifugal compressor which parts of the kinetic energy of the air is transferred into pressure energy. The pressure energy of the air is higher. The air at an increase pressure is delivered to the receiver.

2. OVERALL IMPELLER DESIGN OF CENTRIFUGAL COMPRESSOR

The pressure ratio can be calculated from the equation,

$$r_p = \frac{p_2}{p_1} \quad (1)$$

Where, r_p = pressure ratio,
P_2 = impeller outlet pressure
P_1 = impeller inlet pressure

The law of thermodynamic fundamental of compressor operation is the ideal gas law,

$$PV = mRT \quad (2)$$

Where, P= pressure,
V= volume,
m= mass
R= specific gas constant,
T= temperature

$$R = \frac{R_o}{M_w} \quad (3)$$

Where, R_o = universal gas constant,
M_w = molecular weight

For polytropic process, the general form of the thermodynamic head is,

$$pv^n = c \quad (4)$$

$$H = mRT_1 \frac{n}{n-1}\left[\left(r_p\right)^{\frac{n-1}{n}} - 1\right] \quad (5)$$

Where, H = head of the impeller
T_1 = inlet temperature of impeller
n = polytropic index

The rotational speed is,

$$N = 0.9 \times ratedspeed \quad (6)$$

Where, N = rotational speed

2.1 Dimension of impeller inlet

The shaft diameter is given by

$$d_s = \sqrt[3]{\frac{16T}{\pi\sigma_s}} \quad (7)$$

Where, T= torque, d_s= shaft diameter,

σ_s = slip factor

The eye diameter is given by

$$\frac{\pi}{4}d_0^{\,2} - \frac{\pi}{4}d_h^{\,2} = \frac{Q}{v_0} \quad (8)$$

$$d_o = \sqrt{\frac{4Q}{\pi v_0}} + d_h^{\,2} \quad (9)$$

Where, Q= flow rate, d_h= hub diameter,

v_o= absolute velocity

The vane inlet diameter is greater than the impeller eye diameter. The inlet Mach number is calculated by the following equation,

$$M_1 = \frac{V_1}{\sqrt{\gamma R T_1}} \quad (10)$$

Where, M_1 = inlet Mach number

V_1 = inlet velocity

T_1 = inlet temperature

Speed of sound of gas is given by

$$a = \sqrt{k \times g \times R \times T_1} \quad (11)$$

Where, a= speed of sound,

g= 9.81 m/s^2

For compressible fluid, the impeller inlet hub Mach number is 0.2 to 1 as limited in Rama S.R. Gorla (2003). The assumed of mach number is 0.32. The impeller absolute velocity equation is given by

$$v_0 = M \times a \quad (12)$$

Where, M= Mach number

The air flow is axial direction and no pre whirl. So v_1=v_{f1}. Impeller inlet width is given by

$$b_1 = \frac{Q}{\pi \times v_1 \times d_1 \times \varepsilon_1} \quad (13)$$

Where, b_1= width

d_1= impeller inlet diameter

ε_1 = thickness factor (0.8 to 0.9)

Impeller inlet velocity is given by

$$U_1 = \frac{\pi d_1 N}{60} \quad (14)$$

Where, U_1= inlet velocity

N = rotational speed

2.2 Dimension of impeller outlet

Impeller outlet diameter is given by

$$d_2 = \frac{60 \times \sqrt{H \times g}}{\pi \times n \times \sqrt{k'}} \quad (15)$$

Where, d_2= outlet diameter

The value of v_{f1}/v_{f2} is unity.

$$v_{f1} = v_{f2} \quad (16)$$

Where, v_{f1} =axial flow velocity at inlet

v_{f2} =axial flow velocity at outlet

The outlet width is given by

$$b_2 = \frac{Q}{\pi \times v_2 \times d_2 \times \varepsilon_2} \quad (17)$$

Where, b_2 = the outlet width

v_2= the outlet velocity

d_2 = outlet diameter

Q = flow rate

The outlet vane thickness is given by

$$\varepsilon_2 = \frac{\pi \times d_2 - \frac{z \times t}{\sin\beta_2}}{\pi \times d_2} \quad (18)$$

Where, ε_2 = outlet vane thickness factor

β_2 = outlet blade angle

t = thickness

Z = number of blade

The outlet Mach number is calculated by the following equation,

$$M_2 = \frac{V_2}{\sqrt{\gamma R T_2}} \quad (19)$$

Where, M_2 = outlet Mach number

V_2 = the outlet velocity

T_2 = outlet temperature

2.3 Enthalpy and Efficiency of Centrifugal Compressor

The slip factor is given by

$$\sigma = \frac{v_{\omega_2}}{U_2} \quad (20)$$

Where, σ = slip factor,

v_{ω_2} = whirl velocity at outlet

U_2 = outlet speed

The number of blades is given by

$$\sigma = 1 - \frac{0.63\pi}{z} \quad (21)$$

Where, z= number of blade

The compressor efficiency is given by

$$\eta_c = \frac{h_{02s} - h_{01}}{h_{02} - h_{01}} \quad (22)$$

Where, η_c = compressor efficiency

3. DESIGN MODIFICATION OF CENTRIFUGAL COMPRESSOR

Modified specification of centrifugal compressor are given by

Flow rate = 0.13m^3/s
Rated speed=38000 rpm
Inlet pressure= 950.59kPa
Outlet pressure=620.79kPa
Inlet temperature=350k
Outlet temperature=420k
Mass flow rate=1.3kg/s

These specifications are collected from centrifugal compressor for fertilizer plant located in Pathein. The modified compressor is change flow rate capacity, rated speed, Mach number and mass flow rate from original compressor.

4. VELOCITY DIAGRAM OF IMPELLER

Inlet and outlet velocities triangles of centrifugal compressor are shown in Fig 1.

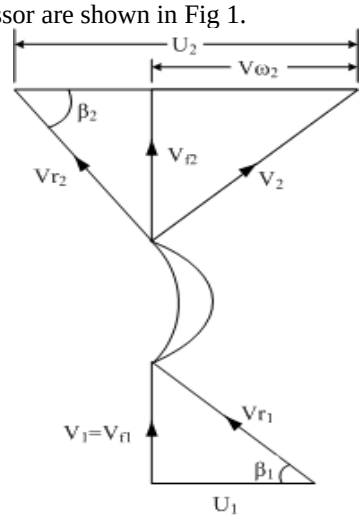

Fig 1 Velocity diagram of a impeller

Inlet blade angle is calculated by the following equation

$$\beta_1 = \tan^{-1}\frac{v_1}{u_1} \quad (23)$$

Where, β_1 = inlet blade angle
V_1= absolute velocity of inlet
U_1= inlet velocity

Out blade angle β_2 is between 55and 75 degrees. The maximum power position, the outlet blade angle is 75 degrees. The air flow outlet angle (α_2) is 21.

The relative velocity is calculated by the following equation

$$V_{r1} = \frac{U_1}{\cos\beta_1} \quad (24)$$

Absolute velocity of outlet is calculated by the following equation

$$V_2 = V_{\omega 2}\cos\alpha_2 \quad (25)$$

Where, V_2 = absolute velocity of outlet

Flow velocity of outlet is calculated by the following equation

$$V_{f2} = V_{\omega 2}\tan\alpha_2 \quad (26)$$

Where, Vf2 = flow velocity of outlet

Relative velocity of outlet is calculated by the following equation

$$V_{r2} = \frac{V_{f2}}{\sin\beta_2} \quad (27)$$

Table 1 Result data of velocity diagram

No	Description	Symbol	Values	units
1	Inlet angle	α_1	21	deg
2	Outlet angle	β_2	75	deg
3	Absolute velocity of inlet	V_1	96	m/s
4	Relative velocity of inlet	V_{r1}	125.337	m/s
5	Inlet velocity	U_1	80.581	m/s
6	Absolute velocity of outlet	V_2	204.439	m/s
7	Flow velocity of outlet	V_{f2}	86.4	m/s
8	Outlet velocity	U_2	223.838	m/s
9	Relative velocity of outlet	V_{r2}	148.957	m/s
10	Whirl velocity of outlet	V_{w2}	185.285	m/s

5. VOLUME OF IMPELLER

Impeller inlet volume is calculated by the following equation

$$p_1 v_1 = mRT_1 \quad (28)$$

The stagnation temperature of inlet and outlet is calculated by the following equation

$$T_{01} = T_1 + \frac{C_1^{\,2}}{2C_p}, T_{02} = T_2 + \frac{C_2^{\,2}}{2C_p} \quad (29)$$

Where, T_{01} = stagnation temperature at inlet
T_{02} = stagnation temperature at outlet

The stagnation pressure of inlet and outlet is calculated by the following equation

$$P_{01} = P_1 \times \left(\frac{T_{01}}{T_1}\right)^{\frac{\gamma}{\gamma-1}}, P_{02} = P_2 \times \left(\frac{T_{02}}{T_2}\right)^{\frac{\gamma}{\gamma-1}} \quad (30)$$

Where, P_{02} = stagnation pressure at outlet
P_2 = static pressure at outlet

Stagnation volume of impeller inlet is calculated by the following equation

$$v_{01} = v_1 \times \left(\frac{p_1}{p_{01}} \right)^{\frac{1}{n}} \quad (31)$$

Where, v_{o1}=stagnation volume of impeller inlet,
P_{01}= stagnation pressure of impeller inlet

Impeller outlet volume and outlet stagnation volume is given by

$$v_2 = v_1 \times \left(\frac{p_1}{p_2} \right)^{\frac{1}{n}}, v_{02} = v_2 \times \left(\frac{p_2}{p_{02}} \right)^{\frac{1}{n}} \quad (32)$$

Where, v_{02}= stagnation volume of impeller outlet,
P_{02}= stagnation pressure of impeller outlet

Table 2 Result data of volume and pressure of impeller

No	Description	Symbol	Values	Units
1	Inlet pressure	P_1	950.59	kPa
2	Stagnation pressure at inlet	P_{01}	1003.2	kPa
3	Outlet pressure	P_2	1620.79	kPa
4	Stagnation pressure at outlet	P_{02}	2009.75	kPa
5	Inlet volume	V_1	0.072	m^3
6	Stagnation volume at inlet	V_{01}	0.069	m^3
7	Outlet volume	V_2	0.047	m^3
8	Stagnation volume at outlet	V_{02}	0.039	m^3

The actual P-V diagram of impeller is shown in Fig 2.

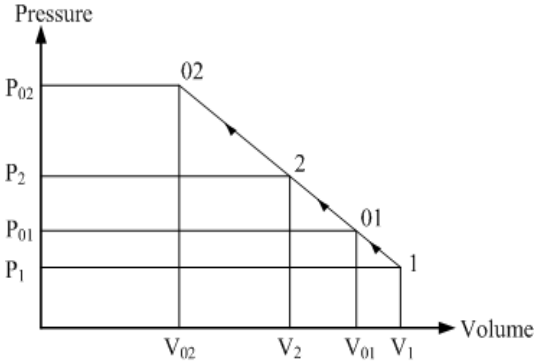

Fig 2 Pressure and volume diagram of impeller

6. VALUE OF MACH NUMBER FOR IMPELLER INLET OF CENTRIFUGAL COMPRESSOR

The following of figures are confirmed the impeller inlet data that present in design. The graph is using the equation 10 and 23.

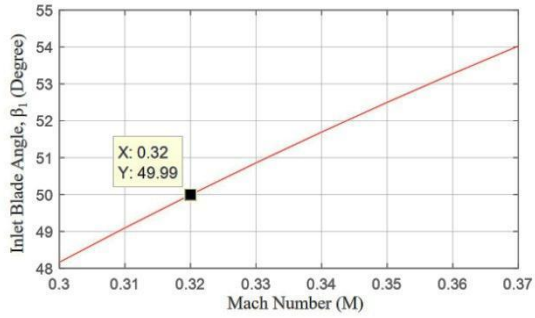

Fig 3 Relation between Inlet blade angle and mach number

The Fig 3, illustrated in the relation between the inlet blade angle and Mach number. There can be seen the inlet blade angle is increase and the Mach number is increase.

The graph is using the equation 10, 14 and 23.

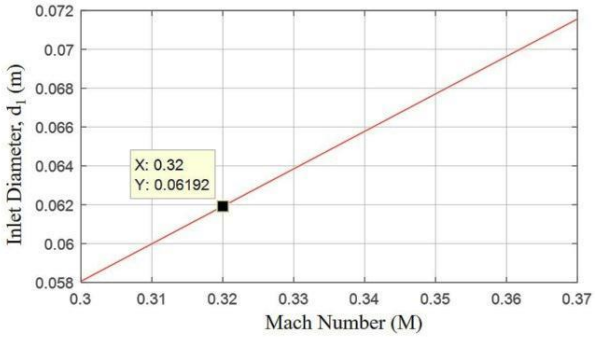

Fig 4 Relation between Inlet diameter and mach number

The Fig 4, illustrated in the relation between the inlet diameter and Much number. There can be seen the inlet diameter is increase and Mach number is increase.
The graph is using the equation 10 and 13.

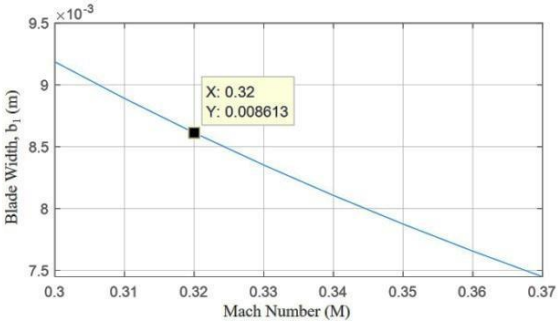

Fig 5 Relation between blade width and mach number

The Fig 5, illustrated in the relation between the blade width and the Mach number. There can be seen the blade width is decrease and the Mach number is increase.

Based on these condition, the Mach number 0.32 is approximately equal to the actual data of the entering impeller of centrifugal compressor. Therefore, the centrifugal compressor impeller design is satisfied for at that point of data.

7. CALCULATION RESULT OF CENTRIFUGAL COMPRESSOR

Table 3 Calculated data of centrifugal compressor

No	Description	Symbol	Values	Unit
1	Head	H	48.313	kJ/kg
2	Torque	T	27	N-m
3	Speed of sound	a	374.5	m/s
4	Mach number at inlet	M_1	0.32	-
5	Mach number at outlet	M_2	0.62	-

Table 4 Comparison for existing and calculating data

No	Description	Symbol	Existing data	Calculated data	Unit
1	Shaft diameter	d_s	0.02	0.019	m
2	Inlet diameter	d_1	0.065	0.062	m
3	Outlet diameter	d_2	0.134	0.125	m
4	Hub diameter	d_h	0.025	0.021	m
5	Eye diameter	d_e	0.06	0.042	m
6	Inlet width	b_1	0.0083	0.008	m
7	Outlet width	b_2	0.0032	0.003	m
8	Number of blade	z	13	13	
9	Efficiency	η	92	95	%

The existing data are greater than calculated data in all condition but the calculated efficiency is greater than the existing efficiency. In centrifugal compressor, the number of impeller blades is equal. So, this condition is reliable.

8. RESULTS OF IMPELLER

The Fig 6 shows the design drawing of the designed impeller. The Fig 7 to 10 shows the velocity distribution and the pressure distribution of centrifugal compressor impeller by using Solid Works software. To run these flow simulations the input data are the rotational speed. The value of impeller inlet and outlet velocity and pressure is nearly equal with numerical value.

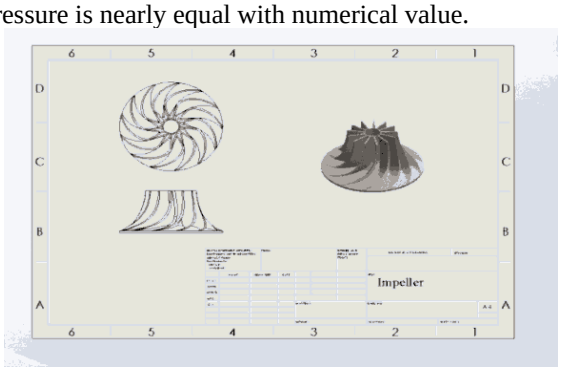

Fig 6 Design drawing of the designed impeller

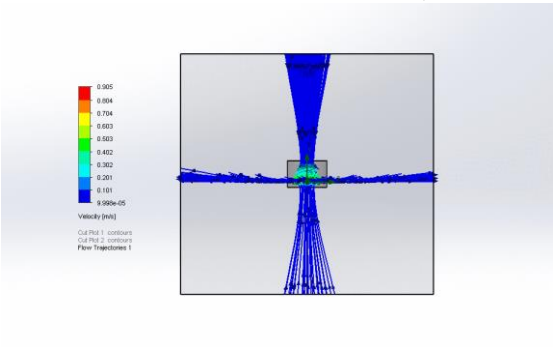

Fig 7 Velocity distribution of the centrifugal compressor impeller (flow trajectories)

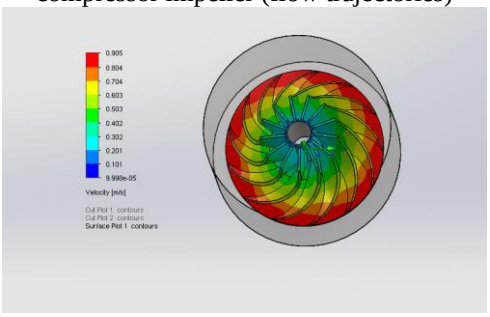

Fig 8 Velocity distribution of the centrifugal compressor impeller (surface plot)

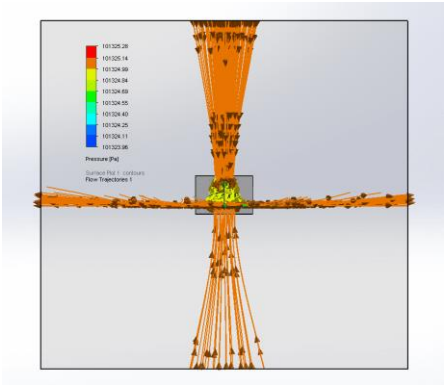

Fig 9 Pressure distribution of the centrifugal compressor impeller (flow trajectories)

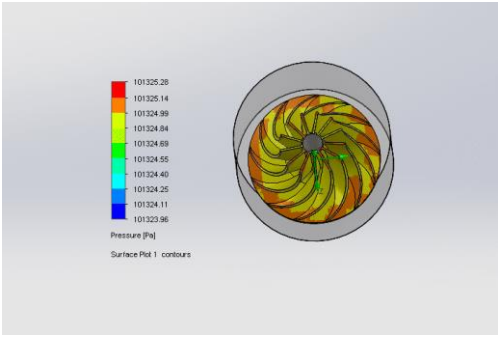

Fig 10 Pressure distribution of the centrifugal compressor impeller(surface plot)

9. CONCLUSIONS

The centrifugal compressor impeller design is calculated in this paper. By using MATLAB, the relation between the impeller inlet of inlet blade angle and Mach number, the inlet diameter and Mach number, the inlet width and Mach number are illustrated. The design of impeller is inlet and outlet

diameter and number of blade and blade width. This paper shows the inlet and outlet velocity triangle and describes the P-V diagram. This paper describes the pressure distribution and velocity distribution by using Solid Works software. The results data are the shaft diameter is 0.019m, the inlet blade angle is 49.99 degree, the inlet diameter is 0.062m, the outlet diameter is 0.125m, the inlet blade width is 0.008m, the outlet blade width is 0.003m and the number of blade is 13 respectively. The efficiency of the centrifugal compressor is 95%. The operation of the centrifugal compressor is reliable. Therefore, the centrifugal compressor is suitable to use in fertilizer plant.

ACKNOWLEDGEMENT

First, the author wishes to acknowledge Dr. Kyaw Thu Ya, Pro-Rector, Pathein Technological University, for giving the opportunity to carry out paper.

The author would like to express her heart felt gratitude to Dr. Aye Aye Thin, Professor and Head, Department of Mechanical Engineering, Pathein Technological University, for her invaluable technological ideas, kindly guidance, patience, immeasurable incentive and help.

Finally, the author wishes to extend our gratitude to her parents and to all teachers that teach her from childhood up to now, all these concerned who have contributed in achieving this paper and to each and every are who assisted in completing this paper.

REFERENCES

[12] HIH Saravanamuttoo, GFC Rogers,H Cohen, PV Straznicky, Gas Turbine Theory (SIX EDITION),2013.

[13] AI-Zibaidy S.N., A purpose design package for centrifugal impellers, Computers and structures, Vol. 55, issue 2, April 1995, pp 347-356.

[14] Xu C., Amano R. S., Empirical Design Considerations for Industrial Centrifugal Compressor, International Journal of Rotating Machinery, Vol. 2012, 15 pages.

[15] Kurauchi S. K. Barbosa J. R., Design of Centrifugal Compressor for natural gas, Vol. 12, 2, 2013, pp 40-45.

[16] Tough R. A., Tousi A. M., Ghaffari J., Improving of the micro turbine's centrifugal impeller performance by changing the blade angles. ICCES, Vol. 14(1),pp 1-22,2010.

[17] Ronald P,Lapina P>E. Estimating Centrifugal Compressor Performance Process compressor technology. Vol-1. McGraw Hill Publications Co, 1982.

[18] H.K. Ludtke, Process Centrifugal Compressor: Basics, Function, Operation, Design, Application, Springer, 2004.

[19] R.C. Reid, J.M. Prausnitz, and B. Poling, The properties of Gases& Liquid, McGraw Hill, 1987.

[20] Rama S.R.Gorla, Turbomachinery Design and Theory, Cleveland State University, Cleveland, Ohio,U.S.A

Flow Simulation of Centrifugal Compressor for Gas Turbine Power Station

Khin Swe Swe Latt[(1)], Thwe Thwe Htay [2)]
[(1)]Technological University (Thanlyin), Myanmar
[(2)]Technological University (Thanlyin), Myanmar

Email: [(1)]khinswe2latt77@gmail.com, [(2)]thwe2htay@gmail.com

ABSTRACT: Centrifugal compressors are compressible flow machine and it is used in small gas turbines. In this study, a 0.162 m diameter centrifugal compressor with a blade outlet width of 0.0021 m has been investigated both theoretical and numerical simulation. The model of centrifugal compressor was first created by using SolidWorks and then simulates the flow analysis. The aim of this study provides an approach to analyze the flow analysis of impeller for centrifugal compressor. The impeller design is based on parameters flow analysis using air as the working fluid. In this design, the impeller blade has exit angle 65º with inlet blade angle 37.74º. So, this compressor is backward-curved blades. The number of blades having 19 equally spaced vanes with the profile is used to improve compressor efficiency. In this study, the theoretical analysis of centrifugal compressor is validated with simulation results. From the analysis, the results confirmed the design to have acceptance performance with regard to maximum and minimum velocity.

KEYWORDS: *Centrifugal compressor, Impeller, Velociy, Diameter.*

1. INTRODUCTION

Compressor are used in many industrial applications. A compressor is a piece of machinery that compresses a fluid, a liquid of a gas that flows in the compressor into greater pressure. Compressors are mostly used in construction, gas turbine power plants, industry and other air conditioning applications. It is a power conversion machines, like pumps and electric motors. Centrifugal compressors are second only to reciprocating compressor in services. However, the centrifugal compressor established its hold on the market in an era of cheap energy when power cost was rarely evaluated. This compressor has been around for quite a long time. Originally, it was used in process applications at relatively low-pressure, high-volume services.

Centrifugal compressor used in small gas turbines. These compressors are the driven units in most gas turbine compressor trains. The function of a compressor is to admit vapor from a low pressure region, compress it and deliver it to high pressure region.

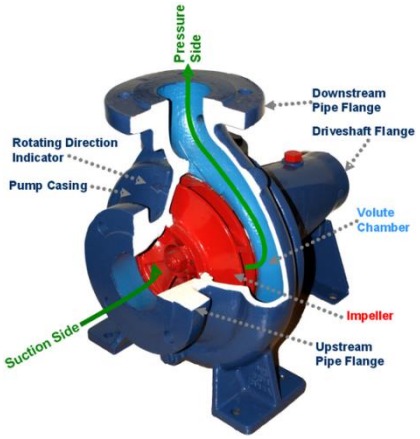

Fig 1 Centrifugal Compressor [8]

Centrifugal compressor consists of a stationary casing containing an impeller that imparts a high velocity to the air and a number of diverging passages, in which air is decelerated with a consequent rise in static pressure. The centrifugal compressor is designed for the most demanding applications where a reliable air supply is required. It is perfect for automotive, commercial and industrial applications. The maximized operating pressure, increased air flow, and extended duty cycle are required.

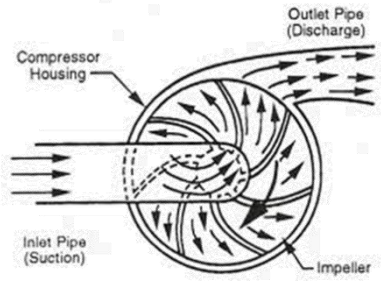

Fig 2 Working Principle of centrifugal compressor [5]

Advantages of the Centrifugal compressor are that it is longer service life than other rotaries and it can increase the pressure for efficient combustion with only one stage. But higher initial cost and air flow is sensitive to change in ambient conditions. However, the airflow for a Centrifugal compressor is much lower than for an axial, and its pressure ratio is generally lower than axial compressor and it is much less effective for creating thrust and less fuel efficient. Hence, it is more

seen in small engines. Centrifugal compressors have two functions: single and multistage

.

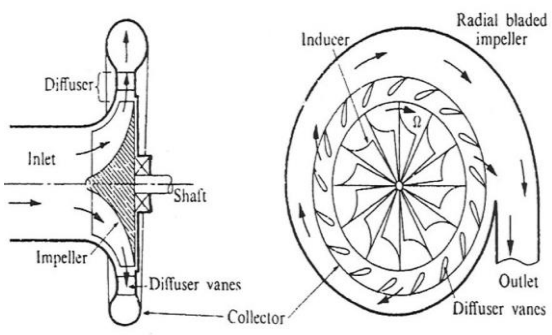

Fig 3 Component of centrifugal compressor [3]

2. THEORETICAL BACKGROUND

The thermodynamics law fundamental to an understanding of compressor operation is the ideal gas law, which is expressed in equation from the follows;

$$Pv = ZRT \tag{1}$$

The general form of the thermodynamic head equation for a polytropic process is

$$H_p = ZRT_1 \frac{n}{n-1}\left[\left(r_p\right)^{\frac{n-1}{n}} - 1\right] \tag{2}$$

This equation drives from integrating the steady-state, steady flow work equation given by:

$$H_p = \int v dp \tag{3}$$

The polytropic process is of form:

$$Pv^n = constant \tag{4}$$

2.1 Impeller Inlet Dimension

The shaft diameter based upon torque alone is given by the equation:

$$D_S = \sqrt[3]{\frac{16T}{\pi S_s}} \tag{5}$$

The eye diameter found from the continuity equation:

$$\frac{\pi}{4} D_o^2 - \frac{\pi}{4} D_h^2 = \frac{Q}{V_o}$$

$$D_O = \sqrt{\frac{4 \times Q}{\pi \times V_O} + D_h^2} \tag{6}$$

The mean diameter of the vane inlet is made slightly greater than the impeller eye diameter.

Speed of sound of gas, a

$$a = \sqrt{k \times g \times R \times T_1} \tag{7}$$

The impeller absolute velocity equation is

$$V_o = M \times a \tag{8}$$

The air enters the impeller eye to tip in the axial direction and prewhirl angle is zero, so that $V_1=V_{f1}$ and is made slightly greater than V_o.

Impeller inlet width, b_1

$$b_1 = \frac{Q}{\pi \times V_1 \times D_1 \times \varepsilon_1} \tag{9}$$

Impeller inlet velocity, U_1

$$U_1 = \frac{\pi D_1 N}{60} \tag{10}$$

2.2 Impeller Outlet diameter, D_2

$$D_2 = \frac{60 \times \sqrt{H_p \times g}}{\pi \times n \times \sqrt{K'}} \tag{11}$$

German turbo compressor practice indicated that with the specified by the meridional velocity ratio V_{f2}/V_{f1}, a value of about unity was desirable, but on larger compressor a value of about ½ appears to give satisfactory results. In this study, compressor size is small. Therefore

$$V_{f2} = V_{f1} \tag{12}$$

The outlet width is expressed by the following equation,

$$b_2 = \frac{Q}{\pi \times V_2 \times D_2 \times \varepsilon_2} \tag{13}$$

2.3 Number of blades

The greater the number of vanes, the smaller the slip, i.e. the more nearly $V_{\omega 2}$ approaches U_2. It is necessary in design to assume a value for the slip factor σ;

$$\sigma = \frac{V_{\omega 2}}{U_2}$$

To find the number of number of blades, the following equation is used.

$$z = \frac{0.63\pi}{\left(1 - \sigma\right)} \tag{14}$$

Where,

H_p : polytropic head, kNm/kg
D_s : shaft diameter, m
D_o : eye diameter, m
D_1 : inlet diameter, m
D_2 : outlet diameter, m
a : speed of sound, m/s
M : mach number
σ : slip factor
z : number of blades

2.4 Specification data

Inlet pressure, P_1 = 1030.766 kPa
Inlet temperature, T_1 = 380 K
Rated speed, N = 45561 rpm
Outlet pressure, P_2 = 1799.6 kPa
Outlet temperature, T_2 = 448 K
Capacity, Q = 0.1275 m^3/s
Air mass flow rate, $\dot{m}$ = 1.5907 kg/s
Shaft diameter, D_s = 0.0254 m
Hub diameter, D_h = 0.028m
Eye diameter, D_o = 0.053m
Inlet diameter, D_1 = 0.054 m
Outlet diameter, D_2 = 0.17m
Inlet width, b_1 = 0.0098m
Outlet width, b_2 = 0.0025 m
Number of vanes, z =19

Centrifugal compressor with this specifications has been installed on Ywama Power Station at Insein Township, Yangon, Myanmar.

2.5 Theoretical Results

Table 1. Calculated Data of Impeller

No	Design Parameter	Sym-bol	Values	Units
1	Polytropic head	H_p	66.7	kNm/kg
2	Torque	T	32.577	N-m
3	Speed of sound	a	390.221	m/s
4	Mach number	M_1	0.3	-
5	Inlet velocity	U_1	103.283	m/s
6	Absolute velocity at inlet	V_1	119.993	m/s
7	Relative velocity at inlet	V_{r1}	158.322	m/s
8	Inlet blade angle	β_1	49	deg
9	Outlet velocity	U_2	346.22	m/s
10	Absolute velocity at outlet	V_2	315.912	m/s
11	Relative velocity at outlet	V_{r2}	132.397	m/s
12	outlet blade angle	β_2	65	deg

Table 2. Comparison of Calculated and Existing Data

	Design Parameter	Sym-bol	Un-it	Calculated data	Actual data
1	Shaft diameter	D_s	m	0.0254	0.0254
2	Hub diameter	D_h	m	0.0286	0.028
3	Eye diameter	D_o	m	0.047	0.053
4	Inlet diameter	D_1	m	0.048	0.054
5	Outlet diameter	D_2	m	0.162	0.17
6	Inlet width	b_1	m	0.0093	0.0098
7	Outlet width	b_2	m	0.0021	0.0025
8	Number of vanes	z	-	19	19

According to the table 2, the impeller of this paper is calculated inlet and outlet diameters and blade width and number of blades. The designed data of impeller inlet in this research are as well as the shaft diameter D_s is 0.0254 m, the hub diameter D_h is 0.0286m, Eye diameter D_o is 0.047m, Impeller inlet diameter D_1 is 0.048m, Impeller outlet diameter D_2 is 0.162m, Inlet width b_1 is 0.0093m, Outlet width b_2 is 0.0021m. All of the calculated data are slightly smaller than the actual data.

3. FLOW SIMULATION FOR IMPELLER

In this study, the SolidWorks simulation is used to analyze the pressure and velocity distribution of centrifugal compressor impeller. The first step of simulation is the user would work with a impeller assembly model in SolidWorks, accessing SolidWorks flow simulation via a menu heading in SolidWorks and follow these steps. The Wizard is selected from the SolidWorks flow simulation menu and firstly chooses

the configuration for the analysis as well as the unit system requirement.

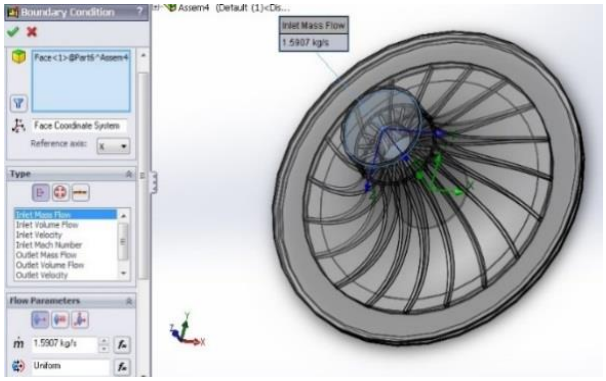

Fig 4 Inlet Boundary Condition

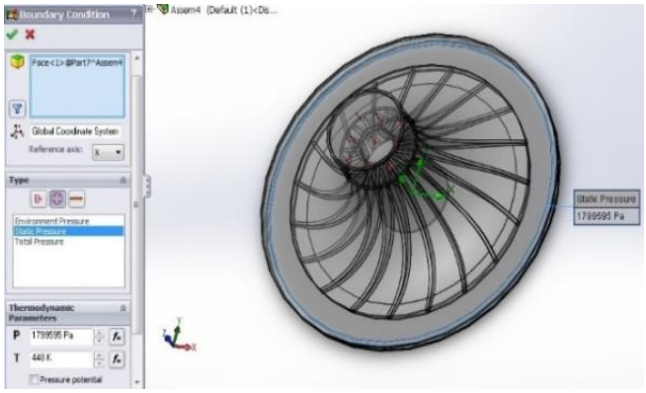

Fig 5 Outlet Boundary Condition

To determine the boundary condition at inlet and outlet of impeller cover, the inlet boundary condition is the inlet mass flow rate and outlet boundary condition is the discharge pressure. Next, choose the working fluid, which in this case is air. The program has a library of commonly used liquids and gases from which to choose. Finally select the resolution of result on a scale from one to eight. The higher the number, the more refined the mesh will be and the more accurate the results.

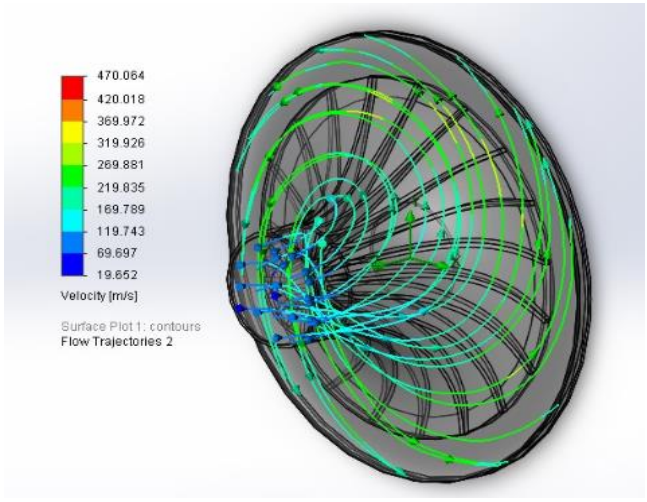

Fig 6 Velocity distribution of centrifugal compressor impeller (flow trajectories)

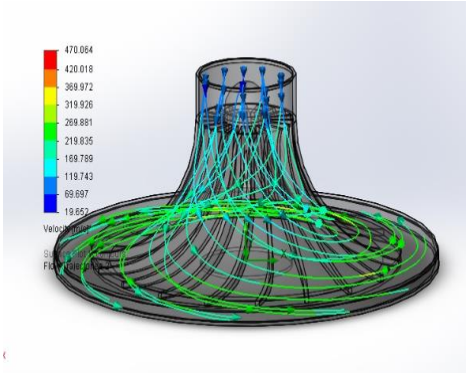

Fig 7 Velocity distribution of centrifugal compressor impeller (flow trajectories- side view)

Fig 6 and 7 show the flow trajectories velocity distribution of centrifugal compressor impeller by using SolidWorks software. The inlet boundary condition is the inlet mass flow rate. The value of inlet mass flow rate is 1.5907 kg/s. The outlet boundary condition is the outlet pressure. The value of outlet pressure is 1799.595 kPa. The theoretical result of impeller inlet velocity V_1 is 117.566 m/s and outlet velocity V_2 is 336.209 m/s. The numerical result of inlet velocity rate is 69.697 to 119.743 m/s and outlet velocity rate is 319.926 to 369.972 m/s. So, theoretical result of impeller inlet and outlet velocity are nearly the same with numerical result.

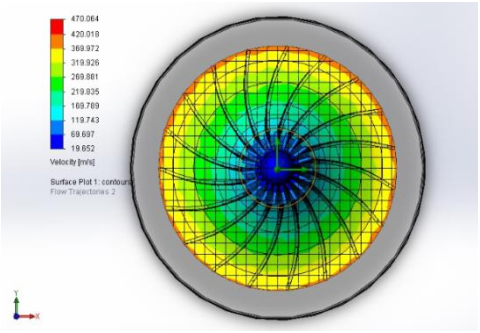

Fig 8 Velocity distribution of centrifugal compressor impeller (surface plots - top view)

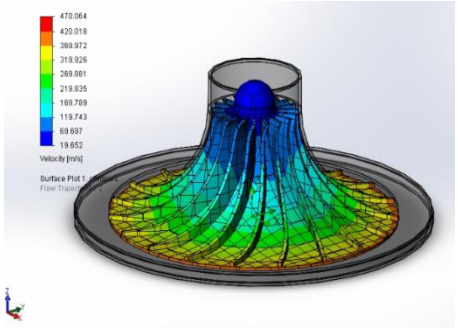

Fig 9 Velocity distribution of centrifugal compressor impeller (surface plots - side view)

Fig 8 and 9 illustrate the surface plots velocity distribution of centrifugal compressor impeller by using SolidWorks software. Mass flow rate and outlet pressure are input data for these flow simulation. The theoretical of impeller inlet and outlet velocity are approximately equal with numerical value.

4. CONCLUSIONS

Centrifugal compressors compress air to raise pressure at high speed. Centrifugal compressor from 'Ywama Power Station' is designed in this paper. The inlet and outlet diameter of impeller, number of blades and blade width were calculated. And then, the theoretical calculation of the inlet and outlet velocity was discussed. Finally, the numerical simulation of the velocity distribution for the impeller is done using SolidWorks software Package. It can be seen that theoretical results of inlet and outlet velocity are nearly equal with numerical results. In this analysis, the design calculation of impeller for centrifugal compressor is satisfied with the existing data.

REFERENCES

[1] Screw Compressor and Axial Compressor. http://www.axial-centrifugalcompressor.com
[2] Nitish Bhushan –IIT Delihi
Tutor-Prof S. Sarkar
[3] McGRAW-Hill, Compressor Handbook, 2001
[4] Meherwan, P. Boyce: Gas Turbine Engineering Handbooks, Part-II.2nd .Ed., New Delhi: Gulf Professional Publishing Co.,2002.
[5] Rama S.R.Gorla, Turbomachinary Design and Theory,Cleveland State University, Cleveland, Ohio, U.S.A 2003.
[6] Beckers, J.: Uses of High-Speed Turbocompressors in Offshore Installations. http://www.Compressor type/cent;/.com.2006
[7] Akhtar, M.S.2001. Selection and Optimization of Centrifugal Compressor for oil gas applications, February 2007
[8] Woodhouse, H., Inlet Conditions of Centrifugal Compressor for Aircraft Engine Superchargers and Gas Turbines, 2006.

Flow Simulation Aimed on Velocity and Pressure Distribution around the Submersible Pump Impeller

Nang Mya Nu Khine Tun(1), Ei Ei Soe(2)
(1)Technological University (Kyaing Tong), Myanmar
(2) Technological University (Dawei), Myanmar

myanukhine@gmail.com

ABSTRACT: Pump technology is a improving technology in the world. The application and use of pumps today are universal. This paper is intended to express about submersible pump which can produce hydraulic energy by using water pressure. The blade design of submersible pump is chosen for this paper because it can widely use in the field of municipal water works, drainage system, power plants, agriculture, irrigation work and many other utility services and industries. In this paper, the design parameters of submersible pump blade were calculated by applying analytical and computational methods. The required design parameters of submersible pump are surveyed from Hlaing River Water Pumping Project (Thapyay Tan). This is the mixed flow pump. This paper relates to design of impeller of submersible pump that can develop a head of 10 m and deliver 68 m^3/min (1.1333 m^3/s) of water at the speed of 730 rpm. In this paper, CFD analysis for flow simulation was done by ANSYS software for velocity and pressure distribution around the blade.The simulation results are quite satisfied when comparing with those from the calculation results. The designed submersible pump impeller can fulfill the requirements of agricultural process.

KEYWORDS: *pump, impeller, CFD, Flow Simulation, ANSYS*

1. INTRODUCTION

A device which lifts water up to a higher level by using mechanical energy is called a pump. It increases the pressure energy of a fluid. The pressure energy is increased when it creates a region of low pressure which is usually lower than the atmospheric pressure near the inlet of the pump and a higher pressure at the outlet of the pump. The low inlet pressure causes the liquid from a low level reservoir to rise up to the pump. The high pressure which is created inside the pump forces the liquid out of the pump and is delivered to the reservoir. [1]

From some external source, the mechanical energy is transferred to the liquid flowing through the pump. Therefore the pump increases the energy of the liquid. This may then be used to lift the liquid and to overcome the hydraulic resistance of the delivery pipe. The pumping system consists of a suction pipe, a pump and a delivery pipe. Pumps are widely used in industry. They provide cooling and lubrication services. They are used to transfer fluids for processing, and to provide the motive force in hydraulic systems. Most manufacturing plants, commercial buildings, and municipalities used pumping systems for their daily operation. In the manufacturing sector, 27 percent of the electricity used by motors are pumps. Basically, in the commercial sector, pumps are used in heating, ventilation, and air conditioning systems to provide water for heat transfer. Municipalities use pumps for water and wastewater removal and treatment. Pumps are also used in land drainage**.** A submersible pump, otherwise called an electric submersible pump, is a device that can be fully submerged in water is shown in Figure 1. The motor is sealed and close-coupled to the pump body. A submersible pump pushes water to the surface. This is done by converting rotary energy into kinetic energy and then into pressure energy. It connects pump body and motor into a whole one. It is suitable for conveying liquid with slurry, solid particles of gravel, cinders, tailings and ground water for irrigation, municipal water use, etc. There are a variety of choices of submersible pump. They can be chosen according to different situations. For instance, some special work may need submersible sewage pump.

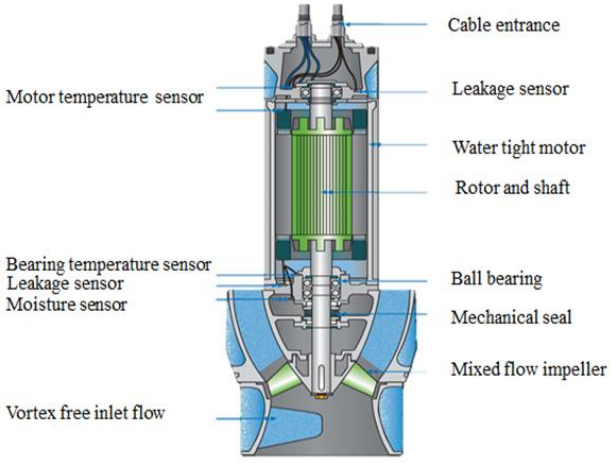

Fig.1.Submersible pump

The submersible pumps used in electric submersible pump installations are operating in a vertical position.. Submersible pump produced liquid, after being subjected to great lift forces caused by the high rotational speed of the impeller, lose their kinetic energy and where a conversion of kinetic to pressure energy takes place. The shaft of the pump is connected to the protector by a mechanical coupling at the bottom of the pump. Well fluids enter the pump through an intake screen and are lifted by the lift forces causes by the impeller.

One main advantage to a submersible pump is that it never has to be primed, because it is already submerged in the fluid. Another advantages is that submersible pumps are very efficient because they don't really need to spend a lot of energy in moving water into the pump. The water pressure saves a lot of energy by pushing the water into a submersible pump.

However, there are a few disadvantages in using submersible pumps. The seal can become corroded with time. When this happens, water seeps into the motor, it cannot be used until it is repaired. The seal makes the submersible pump quite difficult to get at for repairs. [2]. This would cause the pump to leak, eventually corroding the internal components and causing it to fail For the pump casting, cast iron is the generally preferred material in most water and waste water pumping application.

2. DESIGN METHODOLOGY

In this paper the designs of the submersible pump impeller blades are based on blade element theory.[4]The design specifications of the impeller blade are pump flow rate (Q) = 1.1333 m^3/s, suction lift (H) = 10m, rotational speed (N) = 730 rpm and input power (p) = 160 kW. In the present case, the submersible pump impeller is divided into ten portions from hub to tip according to blade element theory.

The specific speed is interpreted as the speed at which a geometrically similar model impeller produces unit capacity, unit head and closely associated with the impeller profile proportions. The specific speed can be calculated in this equation.

$$N_s = \frac{N\sqrt{Q}}{H^{\frac{3}{4}}} \quad (1)$$

The velocities of the incoming fluid together with the flow velocity of rotation determine the pitch distribution of the impeller. The flow velocity of the impeller can be calculated by the following relation.

$$v_z = \frac{Q}{A} \quad (2)$$

The relative velocity at inlet of the blade can be calculated in this equation.

$$v_{r1} = \sqrt{U_{mean}^2 + v_z^2} \quad (3)$$

Outlet relative velocity from the impeller blade can be calculated as follow.

$$v_{r2} = \sqrt{v_z^2 + v_{B2}^2} \quad (4)$$

In order to compute the design of impeller blade using blade element theory, the airfoil performance of the blade in term of lift and drag coefficient is necessary. In this paper, NACA 2412 is selected for blade profile due to its maximum lift drag ratio.

For selection of airfoil, lift and drag ratio has been computed in various angles of attack. The result data for angle of attack are shown in table 1. The present study use NACA 2412 which is an optimum condition of the airfoil performance in terms of lift and drag coefficients found in this condition. Maximum lift and drag ratio was at angle of attack of 6.15 degree.

Table 1. Result Data for Angle of Attack

Angle of attack,α	Lift coefficient,C_L	Drag coefficient,C_D	Lift drag ratio,L/D
-8	-0.6128	0.03759	-16.52
-7	-0.5227	0.03164	-16.32
-6	-0.4289	0.02756	-15.56
-5	-0.3279	0.02446	-13.4
-4	-0.221	0.02234	-9.893
-3	-0.1185	0.02095	-5.659
-2	-0.01185	0.02002	-0.5584
-1	0.09865	0.0197	5.007
0	0.2054	0.01979	10.38
1	0.3137	0.02032	15.44
2	0.4216	0.02135	19.75
3	0.5294	0.02284	23.18
4	0.6352	0.02475	25.66
5	0.7405	0.02725	27.17
6.15	0.8619	0.03098	27.82
7	0.9385	0.03421	27.43
8	1.032	0.03891	26.53

It is assumed that the forces on a blade element can be calculated by means of two dimensional airfoil characteristics using an angle of attack determined from the incident resultant velocity in the cross-sectional plane of the element; the velocity component in the span-wise direction is ignored. Three-dimensional effects are also ignored.Figure 2 shows all the velocities and forces relative to the blade chord line at radius r.

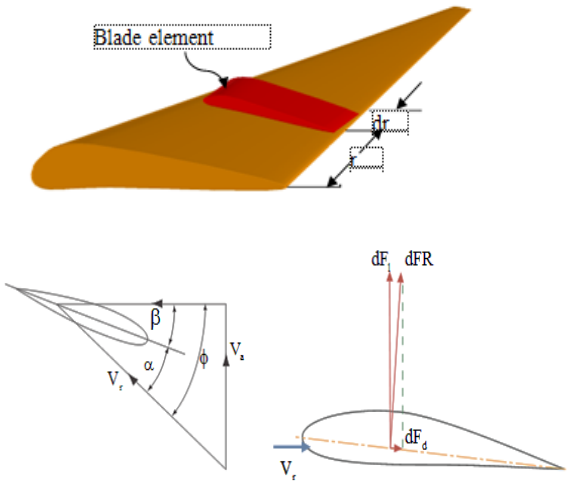

Fig.2. Blade element velocities and forces[4]

The lift force on each blade, normal to the direction of the relative velocity is therefore,

$$dF_L = \frac{1}{2}\rho c dr v_r^2 C_L \quad (5)$$

And the drag force parallel to the relative velocity is

$$dF_D = \frac{1}{2}\rho c dr v_r^2 C_D \quad (6)$$

The resultant of d_L and d_D gives the aerodynamic force dF, which can be solved into the resultant force dF_R.

$$dF_R = \sqrt{dF_L^2 + dF_D^2} \quad (7)$$

In the present case, the submersible pump impeller is divided into ten portions from hub to tip according to blade element theory. The design of the impeller is based on airfoil profiles and lift-drag forces are exerting on airfoil profile. The thrust force for section 1 can be calculated by using this equation.

$$d_F = dF_L \cos\varphi + dF_D \sin\varphi \quad (8)$$

The area of the blade element can be calculated by this equation

$$A_b = c \times dr \quad (9)$$

Then, the pressure acting on each blade element can be calculated from the following equation.

$$P = \frac{dF_R}{A} \quad (10)$$

The result data of blade profile for ten sections are shown in table 2.

Table 2. Result Data of Blade Profile for Ten Sections

No.	radius	Speed ratio	Ø	β	Ø mean	d_L	d_D	d_F	d_T	d_{FR}	c
1	0.12	0.63	38.3	32.2							
					35.9	224	8.1	278	25	224.3	0.1141
2	0.15	0.83	33.6	27.4							
					31.6	331	11	291	27	330.9	0.1141
3	0.19	1.02	29.6	23.4							
					27.9	461	16	301	29	462	0.1141
4	0.22	1.21	26.3	20.2							
					25	617	22	308	31	617.8	0.1141
5	0.26	1.4	23.6	17.4							
					22.5	797	28	314	32	798.3	0.1141
6	0.29	1.59	21.3	15.2							
					20.4	1002	36	318	33	1003.4	0.1141
7	0.33	1.79	19.4	13.3							
					18.7	1232	44	321	33	1233.2	0.1141
8	0.36	1.98	17.8	11.7							
					17.2	1486	53	324	34	1487.7	0.1141
9	0.39	2.17	16.4	10.3							
					15.9	1765	63	326	34	1766.7	
10	0.43	2.36	15.2	9.14							
					14.8	2069	74	327	35	2070.5	
11	0.47	2.55	14.2	8.11							

3. NUMERICAL ANALYSIS FOR FLOW AROUND IMPELLER

3.1 Geometry Modeling of Impeller

Based on turbomachinery theory concepts, the blade impeller with flow velocities was designed. After that, the airfoil section which will be used in the impeller blade was selected. The numerical analysis on the flow around impeller blade was conducted in ANSYS CFX. Before conducting simulation, the blade model had to be designed in SolidWorks. First of all, the selected NACA airfoil was plotted in Solid Works as shown in figure 3.

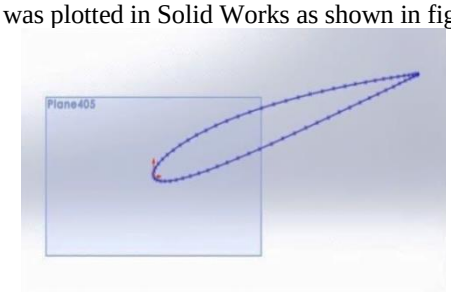

Fig.3. Airfoil or Hydrofoil Section of the Impeller

After setting hydrofoils, the impeller blade was drawn according to its length and the impeller's diameter which came from the hub-tip ratio of the submersible pump. The three dimensional impeller blade profiles were shown in the figure 4.

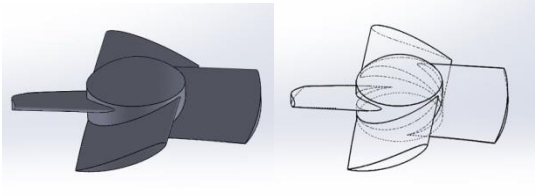

Fig.4.Submersible Pump Impeller Profile

3.2 Defining Domain

As shown in figure 5, the domains of the numerical model were identified. Water will flow through the impeller inside the casing. The type of the fluid has to be defined and the water is the fluid domain at this point. Impeller is the solid domain and the material is steel. After defining domains, the boundary conditions had to be defined. Inlet conditions (0 Pascal). Outlet mass flow rate is 1133 kg/s according to the design requirement specification. The casing is the wall with no slip condition. The impeller has the rotation of 730 rpm according to the design input data. Then, the flow velocity could be investigated within the limitation of the boundary conditions.

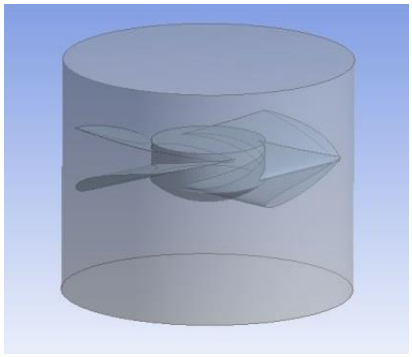

Fig.5. Domains and Boundry Conditions of the Numerical Model

3.3 Grid Generation or Meshing

In ANSYS CFX, there are the meshing tools designed for a specific application such as Turbo Grid, Ice Pak and Air Pak. In this numerical model, ICEM model was used for grid generation as shown in figure 6.

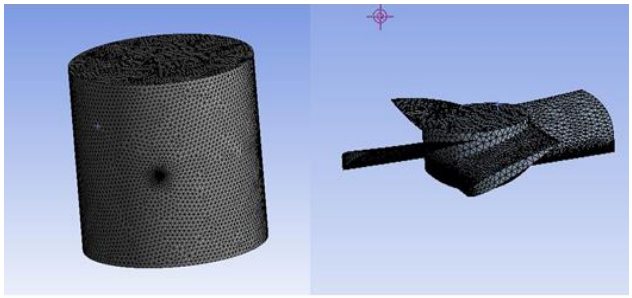

(a) (b)

Fig.6. Meshing of the Model (a) Fluid Domain Meshing

(b) Solid Domain Meshing

3.4.Pessure Distribution of the impeller blade

In figure 7, it can be seen that the pressure distributions respected to their locations. These pressure distributions should meet the good agreement with the calculation results because the calculation was based on the blade element theory which is the common theory in determining the forces and pressures on the airfoil (or) hydrofoil blade. In the figure, the pressure distribution was gradually greater from the root of the blade to the tip of the blade. In blade element theory, the pressure distribution is the largest at the tip and the lowest at the root. Therefore, the simulation results were satisfied with the literature of the blade theory.

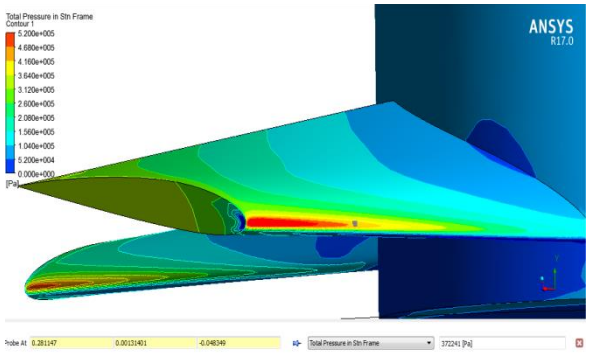

Fig.7. Pressure Distriution around the Impeller

The total pressure distribution on impeller was shown in Figure 8.

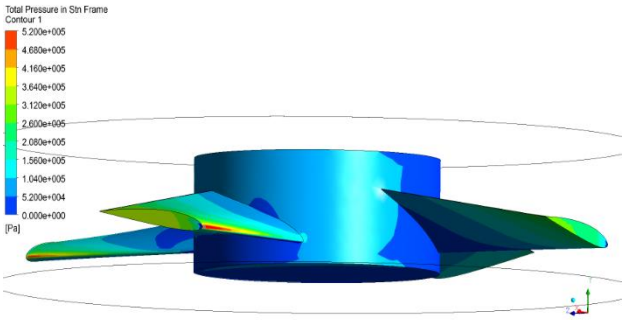

Fig.8. Total Pressure Distribution around the Impeller

3.5. Flow Velocity Distribution around Impeller

Not only the pressure distributions but also the relative (resultant) velocity values were investigated on each section of the impeller blade in the simulation model. The velocity flow was checked in the form of streamline in ANSYS CFX. As shown in the figure 9, the flow profiles in streamline form can be seen in two regions which are solid domain and fluid domain.

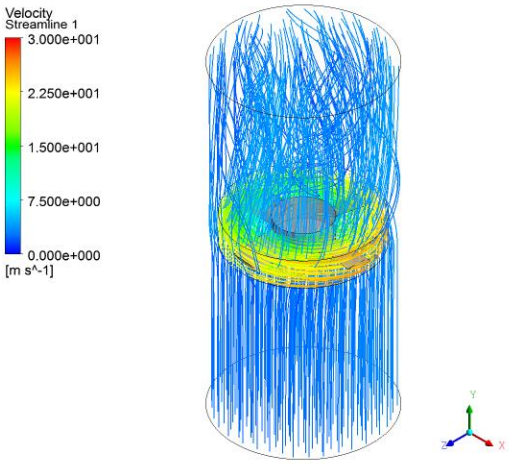

Fig.9. Velocity Streamlime through the Impeller

According to figure 10, it can be seen that velocity distribution at the upper surface of impeller is more than the lower surface of impeller because of swirl velocity

occurred between the end of guide vane and upper surface of runner.

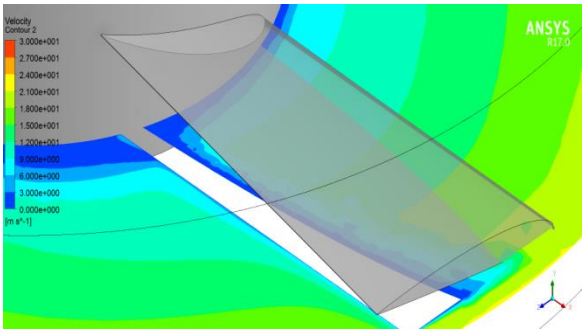

Fig.10. Velocity Countor for Impeller

In simulation model, there are two main velocity components which are necessary to be investigated. They are axial flow velocity and relative velocity around the impeller. In the figure 11, the relative velocity on the section plane was shown. Regarding to the literature theory, the blade relative velocity will increase from the root to tip. In the visualization figure, the velocity flow regions were showing the agreement with the literature background.

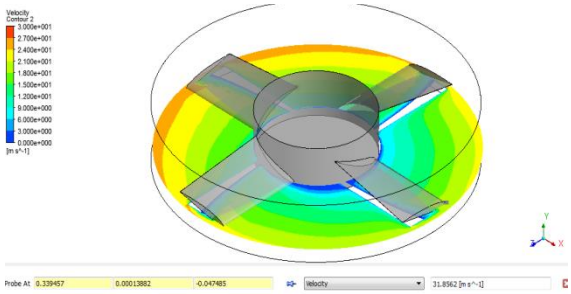

Fig.11. Relative velocity through the Impeller

In numerical simulation, the relative velocities and pressures around the impeller blade were investigated. The velocities and pressure distributions for ten sections on the impeller were calculated by applying the blade element theory. Then, in ANSYS CFX, the velocities and pressure distributions around the blade profile were investigated.

The simulation results and the calculated results for relative velocity are compared in the table 3 . According to the resultant velocity table, the error percentages were under 15% between the calculation results and the simulation results. Therefore, the results of the calculation and simulation could reach the design satisfactory according to the theoretical design calculation and the numerical simulation model in ANSYS CFX.

Table 3. Comparison of the Calculated Relative Velocity with Simulation Results

X (m)	Y (m)	Z (m)	Simulation V_r(m/s)	Calculation V_r(m/s)	Error %
0.15	0.003	-0.05	9.9276	11.41	14.9
0.16	0.003	-0.05	12.721	13.86	8.95
0.17	0.003	-0.05	15.7391	16.38	4.13
0.17	0.003	-0.05	18.9424	18.94	0.012
0.21	0.003	-0.06	20.1186	21.53	7.02
0.22	0.001	-0.04	24.108	24.14	0.137
0.25	0.001	-0.04	25.1286	26.76	6.49
0.28	0.001	-0.47	29.0138	29.39	1.31
0.31	0.001	-0.04	31.1475	32.03	2.83
0.33	0.001	-0.04	31.8604	34.67	8.82

The comparison of the calculated pressure distribution results with simulation results are shown in the table 4. In the table, the total pressures were collected according to their locations in X, Y and Z directions. Regarding to the pressure distributions in each section, it was found that there were no significant differences between the pressure values of the calculation and simulation.

Table 4. Comparison of the Calculated Pressure Distribution with Simulation Results

X (m)	Y (m)	Z (m)	Simulated Pressure (Pa)	Calculated Pressure (Pa)	Error %
0.15	0.15	-0.15	56164.5	56192.2	0.05
0.16	0.05	-0.04	82977.4	82863.7	0.14
0.17	0.01	-0.04	115931	115709	0.19
0.17	0.01	-0.04	154152	154728	0.37
0.21	0.02	-0.04	199084	199922	0.42
0.22	0.01	-0.04	254214	251289	1.16
0.25	0.01	-0.04	309815	308830	0.31
0.28	0.01	-0.04	372241	372546	0.08
0.31	0.01	-0.04	443848	442435	0.31
0.33	0.03	-0.04	521894	518498	0.65

Table 5. Nomencluture

Symbol	Description	unit
N_s	specific speed	rpm
v_z	flow velocity	m/s
ω	angular velocity	rad/s
v_{B2}	rotating blade velocity	m/s
v_{r2}	relative velocity	m/s
α	angle of attack	degree
d_F	thrust force	N
d_T	tangential force	N
dF_L	lift force	N
dF_D	drag force	N
dF_R	resultant force	N
c	chord length	m
β	blade twist angle	degree
Ø	blade setting angle	degree

4. CONCLUSIONS

The designed pump is based on a head of 10 m and deliver (1.1333 m^3/ s) of water at 730 rpm. It is needed to calculate the diameters and blade angles for various sections of the impeller. To obtain all diameters and all blade entrance and discharge angles, the blade is divided into 10 segments from the base of the hub to the outside diameter of the blade. The results of various vane entrance and discharge angles and vane curvatures, blade dimensions at various sections of profile are described in Table II .After calculating the inlet and outlet dimensions, velocities and angles of the impeller, the inlet and outlet diagrams can be drawn and the impeller must be designed. In this paper, the submersible pump impeller profile is also designed by using SolidWorks software. The calculation procedure to estimate the theoretical performance of a pump is an indispensable tool in pump design. This designed submersible pump can fulfill the requirements of agricultural process and then can improve the pump efficiency. In this study, the submersible pump impeller was designed based on the existing design at the practical site. For methodology, analytical design calculation and numerical validation were conducted. For CFD analysis, ANSYS CFX was applied as a numerical tool. The calculated results were compared with the results from the numerical model and the design was satisfied. The results indicate that the submersible pump impeller could give the necessary performance like the existing design from performance like the existing design from the practical site. This research can be extended to more options such as the optimization of the blade parameters and the optimization of the blade twist angle.

ACKNOWLEDGEMENT

The first of all, the author wishes to express special thanks to Dr. Kyaw Thar Tun, Pro Rector, Technological University (Kyaing Tong), for his kindness and valuable permission to summit the paper. The author wishes to convey her deeply thanks to Dr. Phyu Phyu Tun, professor and Head of Department of Mechanical Engineering, Technological University (Kyaing Tong),, for her valuable guidance, kindly advice throughout the preparation of this paper. The author especially would like to express her deep gratitude, respect and regards for her teacher Dr. Mon Mon Zaw, Professor, Department of Mechanical Engineering, West Yangon Technological University, for her continuous supervision, encouragement, patient and trust on this paper.

REFERENCES

[1] S.L. DIXON AND C. A. HALL " Fluid Mechanics And Thermodynamics of Turbo machinery", Six Edition 2010.

[2] BAKER HUGHES. CERTRILIFT " Handbook for Electrical Submersible Pumping System ",

[3] EBARA Corporation, Tokyo, Japan, November, 1999, "Application of Pumps in Agriculture". Six Edition 1997.

[4] Frank P. Bleier, P.E. "FAN HANDBOOK , Selection,Application and Design",1997.

[5] Gahlot V.K. and Nyiri A., Impeller Pumps, Theory and Design, 1993, M.A.C.T., Bhopal.

[6] R. Ramsay, M. Homan, G. Gregorek, Effects of grit roughness and pitch oscillation on the S809 airfoil, in, The Ohio State University, Columbus, 1995.

[7]Jim-Hyuk Kim and Kwang-Yong Kim, Optimization of Vane Diffuser in a Mixed-Flow Pump for High Efficiency Design. International Journal of Fluid Machinery and Systems Vol. 4, No.1, March 2011.

EXPERIMENTAL INVESTIGATION OF PERFORMANCE OF DIFFUSER INTEGRATED VERTICAL AXIS WIND TURBINE

Thandar Nwe(1), Kyaw Aung(2), Aye Aye Khaing(2)

(1)Department of Mechanical Engineering, Technological University Mandalay, Myanmar
(2)Department of Mechanical Engineering, Technological University Mandalay, Myanmar
(2)Department of Mechanical Engineering, Technological University Mandalay, Myanmar

Email: dr.thandarnwe@tum-mandalay.edu.mm

ABSTRACT: The main goal of wind turbine development is to increase power output of the turbine. One of the methods for promising of wind power output is to increase the effective wind velocity by using an augmentation device around the rotor. The objective of the current experimental study is to explore the effect of an accelerator/diffuser around the rotor of a straight-bladed vertical axis wind turbine (SVAWT). The experiment was conducted to investigate the performance of SVAWT with and without diffuser, and to compare theoretical and experimental results of the proposed system. In this test, The SVAWT of NACA0016 with rotor diameter of 1.02m and cord length of 113mm was used to test its performance by adding two flat plate accelerators on both sides of the rotor. Wind turbine power output has significantly increased by integrating the accelerator to the rotor. Maximum power coefficient of 0.43 has attained at 1350mm separation gap from the view of the upwind side and 250mm clearance between the rotor and the accelerator. It was 1.4 times of the bare turbine power output. The results demonstrate that the flat plate technique can give high increased power to the straight-bladed vertical axis wind turbine.

KEYWORDS: *Straight-bladed vertical axis wind turbine, Wind velocity, Diffuser, Power coefficient, Green energy.*

1. INTRODUCTION

Wind-powered energy generation has encountered massive growth around the world and it is examined as an environmentally and economically ambitious advantage of electric power generation by reducing CO_2 emissions into the atmosphere and meeting the growing demand [K. Pope (2010)]. By World Wind Energy report of 2010, 430 terawatt-hours per year, which is 2.5% of the global electricity consumption, can be generated by wind energy technology. Wind energy is generated from the wind by using wind turbines (energy conversion systems) to convert kinetic energy to electricity.

The power in the wind is varying with the cubic flow velocity to the wind turbine, which results in a huge energy generation increment by a small wind velocity rise. The main goal of wind turbine development is to increase the power output of the turbine. The output performance of the turbine is described by the power coefficient *Cp* which is the fraction of power output extracted from the power in the wind by a wind turbine. According to the Betz limit, the maximum average *Cp* value can be increased by creating higher wind speed, increasing the higher torque extracted by the turbine. A feasible way to improve the power of wind turbines is the application of flow augmenting structures around the turbines. That design sometimes referred as a Diffuser Augmented Wind Turbine (DAWT). The augmented device such as shroud or diffuser integrating turbine gives the power coefficient higher than the Betz limit [Y. Ohya, and T. Karasudani (2010), W. Chong (2013)].

The main principle of the diffuser is to convert the kinetic energy of the approaching flow to the rotor into a pressure rise. This creates the lower pressure level in the rotor wake region and makes to capture greater incoming airflow from a free-stream tube to the rotor [B. Geurts (2010)]. Many previous studies have shown that integrating the diffuser to the wind rotor can give a favorable effect on the performance of the wind turbines. But it is still at research phase and the cost of diffuser integrated wind turbine increases due to design complexity. In this work, straight-bladed vertical axis wind turbine (SVAWT) is considered as a design wind turbine. The principle advantages of VAWTs are that they accept the wind from any direction without yawing. Straight, untwisted and uniform section blades of VAWTs are easy to fabricate and give the performance which is comparable with HAWT, with almost 40% extraction of wind energy [[6] B. Habtamu and Y. Yingxue, 2011]. In order to overcome the few disadvantages of the aerodynamics of a straight-bladed vertical axis wind turbine (SVAWT) and to reduce the cost of complex diffuser design, a very simple augmented wind accelerator integrated SVAWT has been considered in this study. The power outputs of the straight-bladed vertical axis wind turbine with and without diffuser were carried out in a field test experiment.

2. MATERIALS AND METHODOLOGY

2.1 Wind power and power coefficient of wind turbine

According to [AN. Celik (2004), R. Kose (2004)], wind power and wind generator power output can be determined by (1) and (2):

$$P_{wind} = \frac{1}{2}\rho A v^3 \quad (1)$$

Therefore, power extracted by a wind turbine can be expressed as

$$P_{turbine} = \frac{1}{2} C_p \rho A v^3 \quad (2)$$

where, A = Swept area of the rotor (m^2)

V = Speed of freely flowing wind strea(m/s)

The power extracted by turbine from the wind can also be written as product of torque (T) and angular speed (ω) as in (3) [R. Bogateanu, et al. (2014)],

$$P_{turbine} = T \times \omega \quad (3)$$

The power in the wind is directly proportional to the air density ρ (kg/m^3), the swept area of the rotor blades A (m^2) and cubed value of the wind speed v^3 (m/s) while the output of the turbine is calculated by the torque T (N-m) and angular velocity ω (rad/s). The performance of the turbine is defined by the power coefficient *Cp* and it can be calculated by (4) and (5): [R. Bogateanu, et al (2014)],

$$C_P = \frac{P_{turbine}}{P_{wind}} \quad (4)$$

$$C_p = \frac{T \times \omega}{\frac{1}{2}\rho A v^3} \quad (5)$$

2.2 Proposed straight-bladed vertical axis wind turbine integrated with wind accelerator/ diffuser arrangement

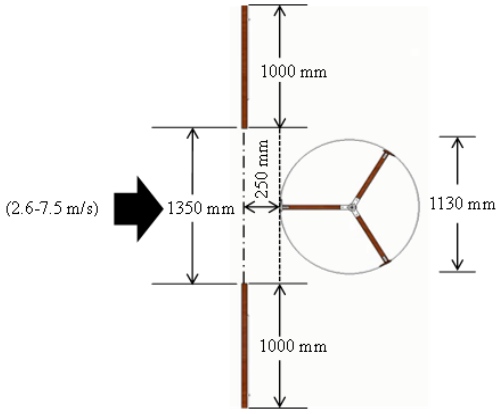

Fig 1. Optimized design specification of flat plate accelerator integrated vertical axis wind turbine

In this study, a pair of simple flat plate is used as an augmentation device (wind diffuser or accelerator) for wind rotor and investigated how to effect of it on the power generation of the SVAWT [T. Nwe (2017)]. Same size of the two flat plate accelerators (2150mm height and 1000mm width) are located in the 90 degree position to the incoming flow at 1350mm of separation gap and 250mm of clearance before the rotor as shown in Fig 1 and Fig 2 [T. Nwe (2018)].

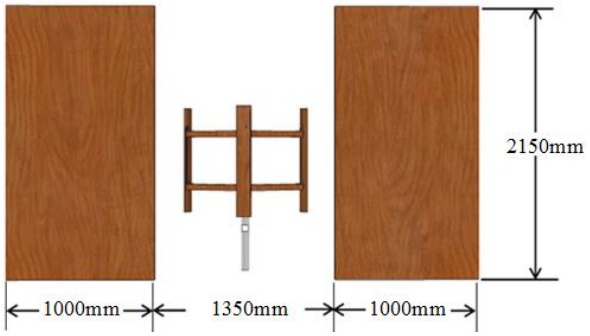

Fig 2. Front view of proposed accelerator integrated vertical axis wind turbine

These optimized data of separation gap and clearance value are obtained from the torque values of simulation results as shown in Fig 3 and Fig 4 [T. Nwe (2018)].

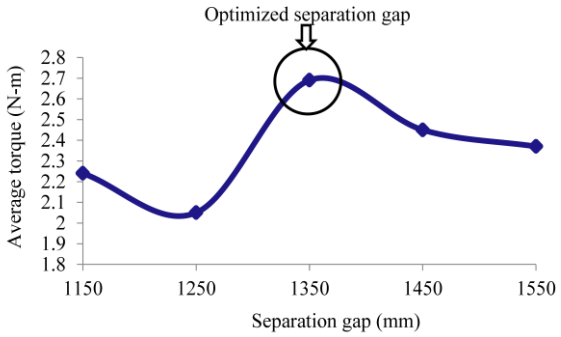

Fig 3. Average torques at different separation gaps

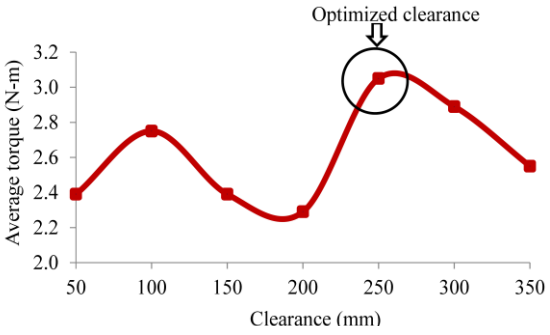

Fig 4. Average torques at different clearances

The concept of this flat plate principle is that the plates change the incoming flow direction to the rotor and accelerates the flow velocity. In this study, the effect of flat plate accelerator on the amount of wind power generation will be investigated experimentally.

3. EXPERIMENTAL SETUP

3.1 Test site

Fig 5 and Fig 6 show the experimental assemblies at the test site. As can be seen from these figures, the site terrain which is near Yankin Hill in Mandalay was nearly flat and the field surrounding the turbine was covered with short grasses. Since VAWT had claimed

that the turbine would generate sufficient power output when mounted at ground level, the turbine was sited near the ground where required design wind speeds meet [Ma Thandar Nwe, Thesis (2018)].

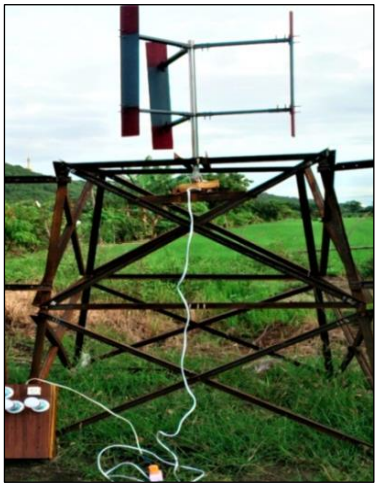

Fig 5. Bare turbine assembly

Fig 6. Diffuser integrated turbine assembly

3.2 Measuring instruments and electric generator

Wind speed is collected with hand-held anemometer and the wind direction is traced harmonically with the rotor facing direction by manually. The output current is measured by clamp meter and the turbine rotational speed is measured by digital display tachometer. The measuring instruments of experimental test are shown in Fig 7.

Fig 7. Measuring instruments for the test

A three-phase permanent magnet generator which has suitable rpm and output power was chosen for the turbine as shown in Fig 8. Generator specifications are number of revolution of 750rpm, voltage of AC 24V and power output of 100W.

Fig 8. Selected permanent magnet generator

4. EXPERIMENTAL PERFORMANCE TEST OF THE TURBINE WITH AND WITHOUT DIFFUSER

The objective of the current experimental study is to investigate the effect of a wind diffuser around the rotor of a vertical axis wind turbine (VAWT). Two different configurations: bare wind turbine case and plate wind diffuser integrated VAWT case were investigated in this experiment as shown in Fig 5 and Fig 6. The experimental time is two months during August and September, 2018. Due to experimental difficulties, it was not possible to measure directly torque value and so only the electric power produced were determined for the wind speeds of 2.6m/s-7.5m/s. As in the previous situation, the electric power produced was evaluated with the aim to determine the coefficient of performance.

For both bare turbine and accelerator/diffuser integrated turbine configurations, the voltage and current from the generator of the wind turbine were measured manually at each wind speed using a clamp meter. All voltage and current were measured and the output power was calculated. The test was carried out from the starting wind speed of 2.6m/s to the rated wind speed of 7.5m/s. In each section of wind speed, the test was performed. The output range including the maximum power output at a given wind speed was examined. When all conditions were changed, the results were recorded after obtaining a stabilized state.

4.1 Comparison of experimental test results on wind turbine performance (with and without diffuser)

The measured data in August and September for the power output of the turbine with and without accelerator are shown in Fig 9 to Fig 12.

Experimental results describe a complete behavior of the total average electrical power produced by wind turbine combined with accelerator and the output results for two months are plotted at various design wind speeds as shown in Fig 9. Then total average power output of the turbine was calculated by using (2) and (3).

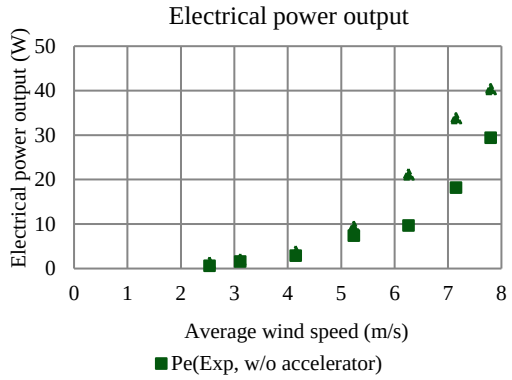

Fig 9. Comparison of total average electrical power output of the turbine for two months with and without accelerator

Total average turbine power output for two months at two different situations are plotted for different wind velocities as shown in Fig 10. The total average torque values for two months are obtained from the turbine power output by using (5) and individual value is plotted against with various wind speeds as shown in Fig 11. Finally performance of the wind turbine was evaluated in terms of the relation between total average power coefficients C_p at each wind speed, describing a performance curve as shown in Fig. 12.

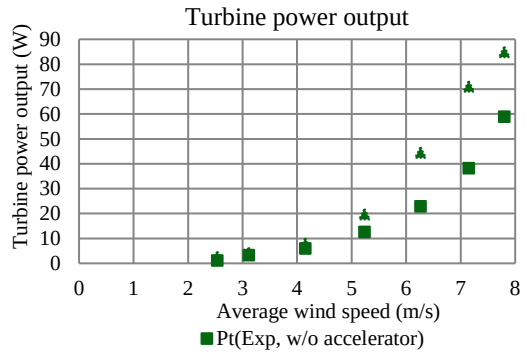

Fig 10. Comparison of total average power output of the turbine for two months with and without accelerator

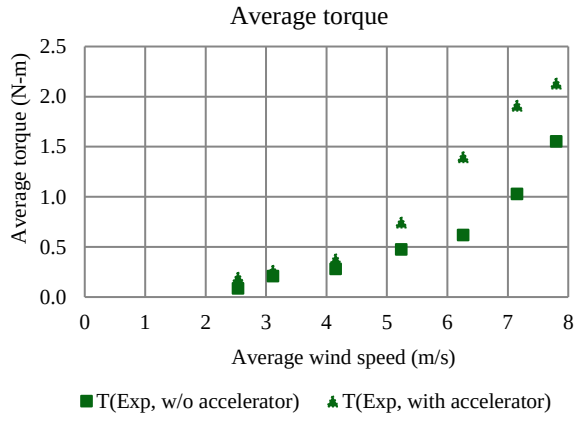

Fig 11. Comparison of total average torque values of the turbine for two months with and without accelerator

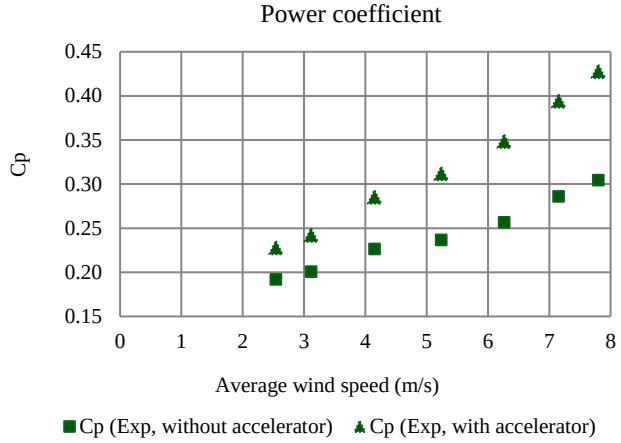

Fig 12. Comparison of total average power coefficient of the turbine for two months with and without accelerator

According to the results, power extracted from the generator for the bare turbine was approximately 29.41W whereas accelerator integrated turbine produces 40.39W. Consequently the power increase can be seen clearly from torque and power output of the turbine. The power coefficient values at different wind speeds for both situations were calculated based on (3). The results indicate that the vertical axis wind turbine with the accelerator/diffuser has the highest coefficient of performance (C_P) of 0.43 while the vertical axis wind turbine without accelerator has C_P of 0.31. In diffuser integrated turbine case, a significant increase in performance occurred in electrical power values. From the results, it is therefore clear that diffuser can increase in electrical power production of wind turbine.

4.2 Comparison of theoretical and experimental results

The comparison of results obtained from theoretical analysis and experimental results is shown in Fig 13 to Fig 16 for with and without accelerator turbine cases respectively.

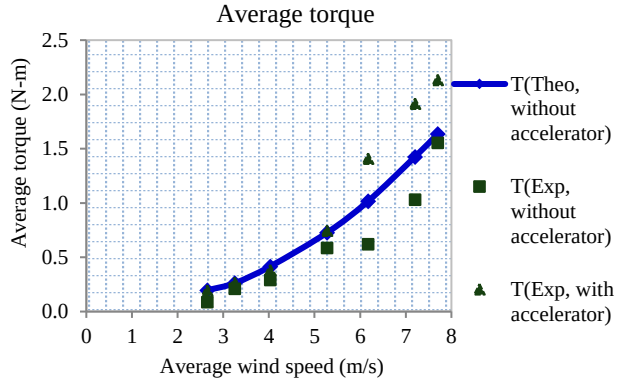

Fig 13. Comparison of average torque values of the turbine with and without accelerator

Fig 13 presents the comparison of theoretical and experimental values of average torque for both without and with diffuser cases. In the bare turbine case, the

highest value is occurred at theoretical result and followed by experimental case. The lowest value attained from the experiment. Similar situation is achieved in the diffuser case. For the bare turbine case, 1.64N-m was achieved in theoretical analysis while 1.55N-m occurred in the experiment at the rated wind speed of 7.5m/s. At the accelerator case, the highest average torque value of 2.14N-m occurred at experimental state at the velocity of 7.5 m/s.

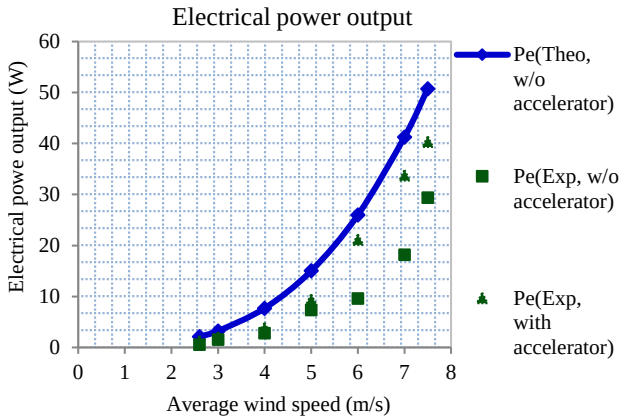

Fig 14. Comparison of electrical power output of the turbine with and without accelerator

The electrical power output results from three different conditions are set against average wind speed as shown in Fig 14. From these results, the accelerator integrated turbine gives higher torque value compared to bare turbine. For the bare turbine case, the electrical power output of 50.14W was produced in theoretical analysis while only 29.41W was generated in the experiment at the rated wind speed of 7.5m/s. In the accelerator integrated turbine case, the highest electrical power output of 40.39W was attained at experimental process at the velocity of 7.5m/s. According to the results, the experimental results are obviously lower than the theoretical analysis. It is because the size and efficiency of selected generator did not match with the system requirement in the experiment.

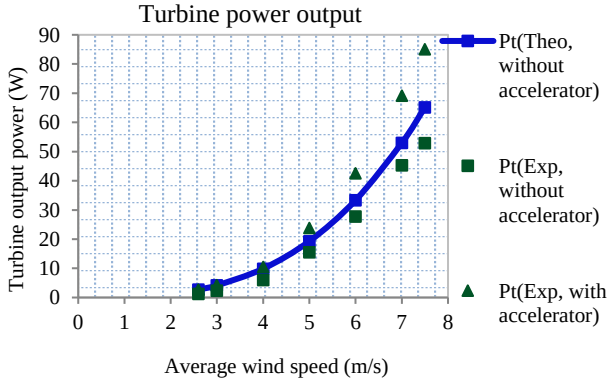

Fig 15. Comparison of power output of the turbine with and without accelerator

Fig 15 shows the turbine power output for the different cases. The experimental maximum turbine power output reached to 85.03W at 7.5m/s by adding accelerator to the turbine. But in the without accelerator case, 59.73W was produced from the experiment at the same wind speed of 7.5m/s.

In terms of power coefficient performance a clear comparison can be given through a confrontation of the data obtained in both situations.

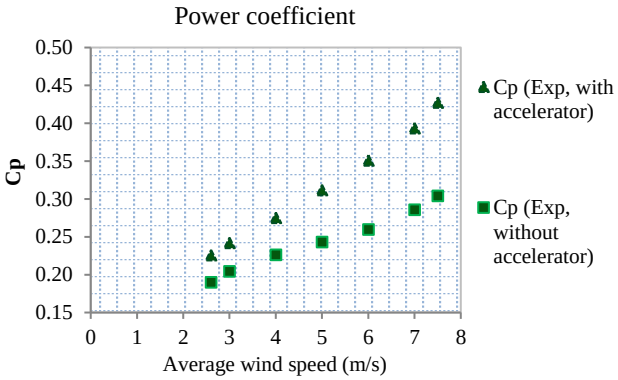

Fig 16. Comparison of power coefficient of the turbine with and without accelerator

It can be obviously seen that the bare turbine efficiency increases to about 1.4 times by adding the flat plates to the turbine. According to the results obtained from the experiment, the maximum output power and the maximum power coefficient for the turbine without accelerator at rated velocity of 7.5m/s attained 29.41W which has maximum C_p value of 0.31. On the other hand, the maximum power of 40.39 W and the maximum power coefficient of 0.43 of the turbine with accelerator were observed at the tip rated velocity of 7.5 m/s. At that time, the theoretical power coefficient value of bare turbine case is 0.32. Therefore it can be seen that the theoretical and experimental results are in good agreement and it reveals that flat plate accelerator can give more power output.

5. CONCLUSIONS

In this study, the field test experiment of straight-bladed vertical axis wind turbine was carried out to understand that the presenting of an augmentation device around the rotor of a VAWT can be favorable to the wind machine energy output. As power coefficient plays a key role in the assessment of wind machines performance, the power outputs as the function of different wind speeds of the turbine were investigated by integrating flat plates at 1350mm specification gap and 250mm clearance in the experiments. According to the results obtained from the experiment, the maximum power output and the maximum power coefficient of the turbine without accelerator were observed at rated velocity of 7.5m/s and attained 29.41W. On the other hand, the maximum power output and the maximum power coefficient of the turbine with accelerator were found at same rated velocity and it produces 40.39W. The accelerator/diffuser achieved 1.4 times of power output increase (depending on the inflow velocity) in both theoretical calculation and experiment. In the calculation, the maximum value of power coefficient *Cp* for the turbine without accelerator was found to be

equal to 0.33 at the rated velocity while *Cp* was 0.46 at accelerator integrated turbine case. In the experimental state, bare turbine gives *Cp* value of 0.31 while accelerator integrated turbine achieved *Cp* value of 0.43. Therefore, it can be proved that the maximum power coefficient increases by a result of implementing the accelerator.

ACKNOWLEDGMENT

The author would like to thank Dr. Kyaw Aung, Professor, Head of Department, Technological University Mandalay, for encouraging submitting this paper. Special appreciation is also credited to Dr. Myat Myat Soe, Professor, Department of Mechanical Engineering, Mandalay Technological University, for her wise guidance during the entire course of this work. The author also would like to record her thanks to Dr. Aye Aye Khaing, Professor, Department of Mechanical Engineering, Technological University Mandalay, for her immeasurable help to this work.

REFERENCES

[1] K. Pope, "Effects of stator vanes on power coefficients of a zephyr vertical axis wind turbine," Renewable Energy, 2010, vol. 35, no.5, pp. 1043-1051.

[2] Y. Ohya, and T. Karasudani, "A shrouded wind turbine generating high output power with wind-lens technology," Energies, 2010, vol.3, no. 4, pp. 634-649.

[3] W. Chong, "The design, simulation and testing of an urban vertical axis wind turbine with the omni-direction-guide-vane," Applied Energy, 2013, vol. 112, pp. 601-609.

[4] B. Geurts, C. Simao Ferreira, and G. Van Bussel, "Aerodynamic analysis of a vertical axis wind turbine in a diffuser," 3rd EWEA Conference-Torque, 2010, European Wind Energy Association.

[5] AN. Celik, "A statistical analysis of wind power density based on the Weibull and Rayleigh models at the southern region of Turkey," Renewable Energy, 2004, vol. 2, no.9, pp. 593–604.

[6] B. Habtamu, Y. Yingxue, "Effect of camber airfoil on self-starting of vertical axis wind turbine," 2011, J. Environ. Sci. Technol, vol. 4, no.3, pp. 302–312.

[7] R. Kose, "An evaluation of wind energy potential as a power generation source in Kutahya, Turkey," Energy exploration & exploitation, 2006, vol. 24, no.4–5, pp. 331–348.

[8] R. Bogateanu, et al., "Reynolds number effects on the aerodynamic performance of small VAWTs". U.P.B. Sci. Bull. 2014, vol. 76, no.1, ISSN 1454-2358, pp. 26-35.

[9] T. Nwe, M.M. Soe, W.W.M. Swe, "Aerodynamic Analysis of Two Different Symmetrical Airfoils for Straight-Blade Vertical Axis Wind Turbine", Proceeding of The 10th AUN/SEED-Net Regional conference on Energy Engineering, YTU, 2017, RCEneE10-13.

[10] T. Nwe, "Analysis of power output and flow characteristic of a small-scaled straight blade vertical axis wind turbine," Proceeding of ICRST (2018), VIIth International Conference on Researches in Science & Technology, 15-16 June 2018, Singapore, ISSN 2463-5979 (online), GICICRST 1804079.

[11] T. Nwe, "Numerical investigation of power output and flow visualization of straight blade vertical axis wind turbine integrated with wind accelerator," International Journal of Scientific and Research Publications, 2018, vol. 8, no. 10, ISSN 2250-3153, pp. 591-608.

[12] Ma Thandar Nwe, "Experimental and numerical investigation of vertical axis wind turbine integrated with wind accelerator," Ph.D. Thesis, 2018 (November), Mandalay technological University, Mandalay.

[13] Takahashi, S., J. Hamada, and Y. Takashi, "Numerical and experimental studies of airfoils suitable for vertical axis wind turbines and an application of wind-energy collecting structure for higher performance," Journal of Wind Engineering, 2006, vol. 108: pp. 327-330.

EXPERIMENTAL INVERSTIGATION OF A DOWNDRAFT GASIFIER BY AGRICULTURAL RESIDUES

Khin War Oo[(1)], Nwe Lin Minn[(2)] , Thu Thu Linn[(3)]
[(1),(2),(3)]Technological University (Hmawbi), Myanmar

Email: [(1)]khinwaroo7@gmail.com

ABSTRACT: Energy demands are increasing consistency because of the use of the fossil fuel energy causing global warming. Biogas is a renewable energy source and easily available, so that several analysis and investigation is going on this area. This paper study present experimental investigation of biomass gasification in downdraft gasifier. Research was done in the real plant at various conditions. Since rice husk was used as fuel in the plant, the effect of fuel moisture on the gasification process performance was examined due high impact on the result. In this paper, analysis the rice husk gasifier for dual-fuel made and their gasification efficiency are calculated. Power output for original diesel engine is 80 kW, and by using dual-fuel engine, output power is 65kW. Dual-fuel engine produces power with nearly 19% decreasing the original engine power. But, in economical point of view, by using dual-fuel engine, daily cost saving is 49628 Kyats.

KEYWORDS: *Biomass gasification, Downdraft gasifier, Experimental research, Economical analysis, Dual-fuel*

1. INTRODUCTION

Biomass is the biological material from living or recently living organisms. Many of the developing countries have growing their interest in bio-fuel development and providing greater access to clean liquid fuels while helping to address the issues such as increase in fuel price, global warming concerns associated with petroleum fuels. Biomass is a carbon, hydrogen and oxygen based. It is used as a good source of power generation. [2].

It must be noted that gasification is cheaper as well as having considerable efficiency compare with non renewable energy sources. Also downdraft gasifiers with throat are known to produce the best quality gas for engines. There are mainly two types of biomass gasifier, which are the fixed and fluidized bed type. The fixed bed gasifiers have been the traditional setup used for gasification, operated at temperature around 1000^{o}C. Among the fixed bed gasifiers, there are three major typesand there are updraft, downdraft and cross-draft gasifiers [3].

Rice husk, a biological form of renewable energy, is the main by-product and residues during the process of milling rice, constituting one-fifth of the paddy by weight. Most rice mill have turned to diesel engine and electric motors as their prime movers for the milling process. [2].

2. THEORETICAL BACKGROUND

2.1 Characteristics of Rice Husk

Each type of gasifier will operate satisfactorily with respect it stability, gas quality, efficiency and pressure losses only within certain range of the fuel properties.

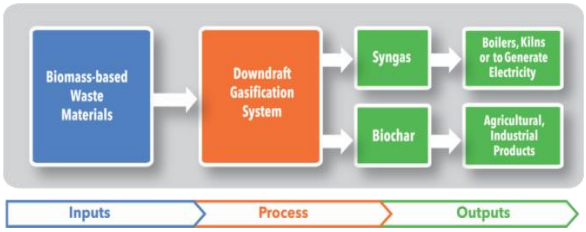

Fig. 1. Gasification system

The most important properties of rice husk are;

- Energy Content: the energy stored in fuel, which released if fuel is burnt to carbon dioxide. This amount of energy expressed by the term calorific value or sometimes, its heating value or energy value. The choice of fuel for gasification will in part be decided by its heating value.
- Moisture Content: the moisture content of the rice husk depends on handling and milling procedures as well as the total storage and the climate. High moisture reduced the thermal efficiency since heat is used to drive off the water.
- Volatile Matter Content: volatile matter is a matter which is volatile when it is heated such a tar, tarry oil etc. As a general rule, if the fuel contain more than 10% volatile matter it should be used in downdraft gasifier. The range of volatile matter content for rice husk is 5.47 to 9.3% based on the moisture content of fuel [4].
- Ash content: ash can use as a variety particularly in updraft or downdraft gasifier. Ash content of rice husk is 15 to 23%.
- Reactivity: the reactivity is an important factor determining the reducing of carbon dioxide to carbon monoxide in a gasifier. Reactivity influences the reactor design and the height of the reduction zone. Reactivity depends on the type of fuel. Rice husk is more reactionary than wood chip, charcoal and coal.
- Bulk Density: bulk density is defined as the weight per unit volume of loosely tipped fuel. Fuels with high bulk density are more advantages. Bulk density varies significantly with moisture content and particle size of the fuel. Range of bulk density is 90 kg/m^3 to 110 kg/m^3[1].

2.2 Composition of Rice Husk

Composition of rice husk depends upon types of rice and different moisture content. This composition of rice husk is shown in Table 1.

Table 1. Proximate Analysis of Rice Husk

No	Example	Proximate analysis(% wt/wt)			
		moisture	Volatile matter	ash	Fixed carbon
1	Bamboo	5.73	74.68	5.55	14.04
2	Rice straw	7.76	65.58	12.44	14.22
3	**Rice husk**	**5.60**	**56.41**	**13.45**	**24.54**
4	Wood	7.49	74.82	6.36	11.33

2.3. Composition of Producer Gas

Gasifying rice husk, that is burning it with limited amount of air, was found to be an effective means of generating heat that can be utilized for various thermal applications and, at the same time smoke problem. Composition of producer gas is shown in Table 2.

Table 2. Gas Composition of Gasification of Rice Husk

Moisture content %	10	20	30	40
	Gas composition of producer gas			
CO	26.1	22.3	18.6	15
CO_2	6.1	8.2	9.5	10.3
H_2	20.6	21.2	21.5	21.2
H_2O	8.6	12.8	18.0	24.0
CH_4	0	0	0	0
N_2	38.1	35.5	32.4	29.5

3. METHDOLOGY

This paper describes the performance of downdraft gasifier by using rice husk. The process started by obtaining information and data needed from Aung Myint Myat rice mill. Calculate the gasification efficiency, fuel consumption rate, engine efficiency and fuel cost rice husk residues and diesel oil for rice mill running six hours per day, to compare the economic saving. And then the electrical power consumption of each of the motors was determined by taking the amperages and voltages using an Ac-clamp meter.

During the test the following data were collected:

1. Start-up time to generate the gas
2. Weight of fuel used
3. Amount of char produced
4. Gas temperature leaving the reactor
5. Air temperature leaving the char box
6. Total electrical consumption (blower, scraper, conveyors)
7. Air and gas velocity

The following parameters were analyzed after each test:

1. Fuel consumption rate
2. Specific gasification rate
3. Power input
4. Power output
5. Percentage char produced

All the results obtained were used in the standard tabulation of the performance of rice husk gasifier.

4. CLASSIFICATION OF GASIFIERS

Theoretically, gasification is the thermo-chemical conversion of organic materials in the presence of limited amount of air , into combustible gases, tar and char produced. The producer gas is formed by the partial combustion of solid bio-mass in a vertical flow packed bed reactor. In the conventional theory of producer gas, gasification reaction takes place in four zones. They are drying, pyrolysis, combustion and reduction zones [4].

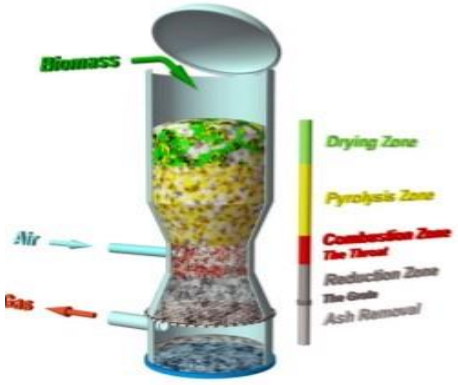

Fig.2. Gasification reaction zones

4.1.Types of Gasifiers

There are mainly two types of biomass gasifiers, which are the fixed and fluidized bed types. The fixed bed gasifiers have been the traditional setup used for gasification, operated at temperature around 1000°C. Among the fixed bed gasifiers , there are three major types and they are updraft, downdraft and cross-draft gasifiers.

The updraft gasifier is the simplest and oldest form of gasifier and is still used for coal gasification, In the updraft gasifier, gas leave the gasifier with high tars vapour which may seriously interfere the operation of internal combustion engine. This problem is minimize in downdraft gasifier. Fig.3. shows the updraft gasifier. [6].

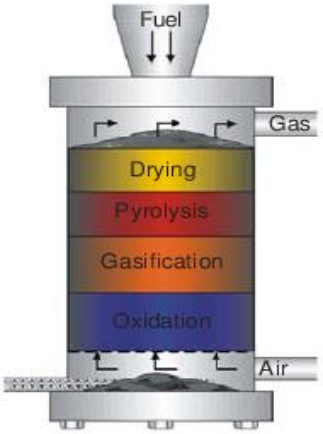

Fig.3.Updraft gasifier

Cross-draft gasifiers are used for charcoal gasification.

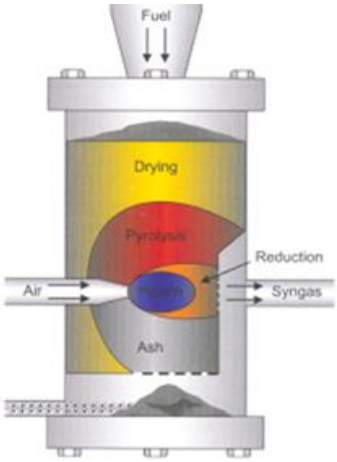

Fig.4. Cross-draft gasifier

The downdraft gasifier has the same mechanical configuration as the updraft gasifier except that the oxidant and product gases flow down the reactor, the same direction as the biomass. In this type air is introduced downdraft flowing packed bed or solid fuels and gas is down off at the bottom. A lower overall efficiency and difficulties in handling higher moisture and ash content are common problems in small downdraft gasifiers [6].

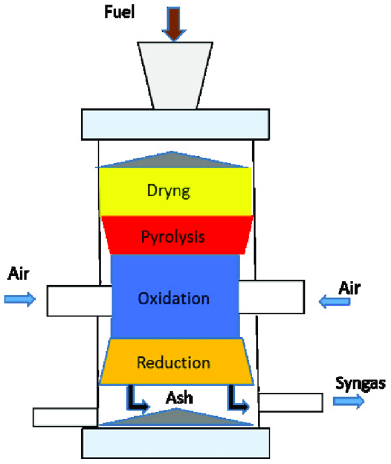

Fig.5.Downdraft gasifier

4.2. Biomass Gasification System

The system consists of downdraft gasifier reactor, cyclone separator, water scrubber, gas cooler, carbon fiber filter, fine filter units and gas damper. The purpose of cyclone is to remove tar and dust from the gas.. The velocity of the contacting liquid both pump and scrubs, the entered gas in an ejector venture scrubber. Producer gas passed through venture scrubber remove ash and to condense tars [8]

.

4.3. Case Study

A case study is made at Aung Myint Myat rice mill located in Thongwa Township, 32 miles from Yangon, which manufactures 1.4 tons of rice per hour, and is constructed in 2004. It consists of one cyclone and two types of gas filter and water scrubber gas cooler. Data from Aung Myint Myat rice mill is shown in Table 3.

Table 3. Data Collected From AUNG MYINT MYAT Rice Mill

Gasifier Type	Throat less, downdraft Length 254 cm, Dia 101.6cm
Engine	8 cylinder, diesel engine
Fuel consumption (dual)	0.67 gal/hr
Fuel consumption (diesel)	4 gal/hr
Rice husk consumption	122.4 kg/hr
Number of cyclone	1 (Dia 194 cm, length 168cm)
Displacement volume (V_d)	20.612 x 10^{-3} m^3
Number of filter	2 (Dia 117 cm, Length 73cm, Length 79cm)
Used source	Rice mill
Rice mill type	Belt type
Cost	18,000,000 Kyats

5.COMPARISON OF DUAL-FUEL AND DIESEL ENGINE

On testing the original diesel engine and dual-fuel engine, the following data are collected, shown in tables.

Table 4. Comparison of Power Output for Diesel Engine and Dual- Fuel Engine

No.	DIESEL ENGINE			DUAL-FUEL ENGINE		
	Volt	Ampere	Output	Volt	Ampere	Output
1	390	160	62.4 kW	380	100	38 kW
2	400	165	66 kW	380	120	45.6 kw
3	410	175	71.8 kW	390	140	54.6 kW
4	420	180	75.6 kW	390	160	62.4 kW
5	420	190	79.8 kW	390	165	64.5 kW

Maximum power output of original diesel engine = 80 kW
Maximum power output of dual-fuel engine = 65 kW
Percentage of power reduced = 19%

In this comparison, is made on the same constant speed of 1200 rpm, and the same volumetric efficiency 51.53%.

Volumetric efficiency (η_v) can be calculated from the following data:
Four stroke diesel engine, engine speed N_e = 1200 rpm
No: of crank shaft revolution, n_r = 2
Displacement volume (theoretical volume of the engine cylinder , V_d = 20.612 x 10^{-3} m^3
Air mass flow rate, m^0 = 0.078 kg/sec
Density of air, $\rho_a = 1.225 kg/m^3$

Actual volume of intake air, $V_a = \frac{m^0{}_a n_r}{N_e \times \rho_a}$

$$V_a = \frac{0.078 \times 2}{1200 \times 1.225} = 10.621 \times 10^{-3} m^3$$

$$\eta_v = \frac{V_a}{V_d} = \frac{10.621 \times 10^{-3}}{20.612 \times 10^{-3}} = 0.5153 = 51.53\%$$

Data collected and calculated for fuel consumption cost of diesel engine and dual-fuel engine. Comparison results are shown in TABLE 5.

Table 5. Comparison of Fuel Cost for Diesel Engine and Dual- Fuel Engine

Engi-ne running time	DIESEL ENGINE		DUAL-FUEL ENGINE			Net saving using rice husk (Kyats)
	Diesel (gal)	Cost (Kyats)	Diesel (gal)	Rice husk (kg)	Total cost (Kyats)	
One day (6 hr)	28	58,800	3.6	1612	9172	49,628

As a result, the monthly saving for fuel cost is 1,488,840 Kyats.

5.1 Environmental Aspect

This technology is considered to be environmental-friendly since it utilizes a renewable energy source in which the by-product is re-usable. With this technology, the annual rice husk production of two million metric tons can be utilized for various thermal energy applications and the by-product can be utilized as variable materials for agricultural and industrial uses. It does not emit harmful gases for it efficiently burns all the gases produced. It has high CO_2 reduction potential and very low back carbon emission, as compare with other thermal generating devices [3].

The char, which is the by-product in the operation of the gasifier, can be used as carbonized rice husk for agricultural use or can be mixed with coal for bio coal pellet production. The ash which is another by-product, can be processed further into locally-produced refractory materials or can be used as raw material in the production of cement-fiber board and geo-polymer products [3].

6. CONCLUSIONS

This paper is studied on the experimental investigation of downdraft gasifier by using agricultural residues (rice husk). Data collected from Aung Myint Myat rice mill, Thongwa Township, 32 miles from Yangon. It was built in 2004, by using dual-fuel engine and producing 1.5 tons of rice per hour. Raw material rice husk is by-product of the rice mill. Experimental analysis is compare of two engines using diesel, dual-fuel. The volumetric efficiency and engine speed is the same. Performance comparison and economic comparisons are made for rice mill, running for 6 hours a day. As a result the output power of diesel engine is 80 kW, and dual-fuel engine is 65 kW. Therefore power reducing is nearly 19%. In economical point of view, daily fuel cost saving is 49,628 Kyats.

The technological can provide more benefits to the user, particularly in terms of conveniences of operation and cost. Likewise, it can provide greater socio-economic advantages to the locality in the production and in the utilization of the technology and to the government as well. It does not required advanced knowledge and high-tech component and equipment in the fabrication. Thus, it can easily built using locally available resources and manpower. It also addresses the environmental aspect of the country and the world. In general, since it is considered a clean technology based on CO_2 emission, which are basically low. Its by-product can be further used as available commodity products.

ACKNOWLEDGEMENT

The author would like to express her special thanks to Prof. Dr. Khin Maung Tin, Steering Committee for Advanced Technological Universities (YTU and MTU), for his useful suggestions and technical guidance. And then the author would like to express her special thanks to the entire person in a rice mill, Myanmar, for giving their data information throughout this research.

REFERENCES

[1] Belonio,A "Continuous-Flow Rice Husk Gasifiers for Medium-Scale Thermal Application" PT Minang Jordanindo Approtech. Jakarta Selaton, Indonesia. 2PP February, 2019.

[2] Higman, C, and Maarten, V. "Gasification" Gulf Professional Publishing, Second Edition, 2008.

[3] Nay Zar Aung, " Conversion of Diesel to producer gas Engine" (ME Thesis) Yangon technological University, 2006.

[4] Rajvanshi, Anil K "Biomass Gasification" Nimbkar Agricultural Research Institute, 2004.

[5] FAO, "Rice Husk gasification Technology in Asia" Papa publication,1991-1992

[6] Albrecht Kaupp," Gasification of Rice husk Theory and Praxis"ISBN3-528-02002-4, 1984

[7] Peter Luby, Ingchem, Bartislava, "Advanced System in Biomass Gasification-Commercial Relity and outlook". International Slovak Biomass Forum, Bratislava, 2003.

[8] Pauchauri, R.K. "Biomass Energy System, Proceedings of the International Conference, New Delhi, 1996.

[9] Tariq, A.S. "Biomass Combustion Systems" ISBN0-84954-385-4, 1994, Natural Resources Institute, London.

[10] Yow Yit Seng, "Industrial management of Rice Husk foe Heat and Power generation", Kuala Lumpur, Malaysia, 1999.

Aggregate Production Planning of a Cement Industry in Myanmar Using Linear Programming

Aung Myo Lwin[(1)], Yin Yin Tun[(2)]
[(1)]Yangon Technological University, Myanmar
[(2)]Yangon Technological University, Myanmar

Email: aungmyolwin.ie@ytu.edu.mm

ABSTRACT*:* Aggregate production planning refers to determining the level of production, inventory, and work force levels to meet demand requirements that fluctuate across the planning horizon. This study conducted an aggregate production planning of a cement industry in Myanmar. Linear programming model is developed to optimize the aggregate production plan for six months time horizon. The objective of this study is to minimize the total cost that includes operation cost, material cost, inventory cost, shortage cost and subcontracting cost. Lingo software was used to solve the linear programming model. The obtained solutions from the model determined production plan, operating days, amount of inventory and shortage and amount of product bought from subcontractors for all six months time horizon.

KEYWORDS: *aggregate production planning, linear programming, Lingo software, optimization, cement industry.*

1. INTRODUCTION

Cement demand in Myanmar was increased year by year in the last decade. In recent years, new cement industries have been established in Myanmar to meet the extended demands of the customers. Now a day, it becomes vital to maximize utilization of the resources and develop effective production plan to keep competitive advantage. Thus, aggregate production planning is important for the cement industry to determine effective production plan for the specific time horizon. Sunil Chopra (2016) defined that aggregate production planning is the process by which companies determine the level of planned capacity, production, subcontracting, inventory, shortages, and even prices within a certain period. The purpose of aggregate plan is to implement a plan that meets demand while minimizing the cost. Aggregate planning determines the total production level at the plant during a particular month. This level of detail makes aggregate planning a useful tool for reflecting on medium-term decisions between approximately 3 to 18 months. In this time period, it is too early to determine the production level, but it is generally too late to establish additional capacity. Therefore, aggregate planning provides a decision on the best use of the company's facilities and resources.

The selected industry is situated in Mandalay division, Myanmar, which has the capacity of 1200 tons/day. The industry operates 24 hours fully a day with three shifts and after fulfilling customer demands, the remaining surplus product is stored in a warehouse as a safety stock for future demands. The current organizational management strategy is to produce continuously without considering customer demand. This study was carried out taking the demand forecast for the next six months for the company and taking into account previous records. According to the company's current production plan, company has to operate 25 days per month. Thus, the current production cost including raw material and inventory cost for next six months is Ks 9883.125 million. As a process industry, the plant continues to operate continuously all the time, so unplanned damage to the plant causes a large investment by the company in the form of maintenance. Due to unplanned outages, valuable production time is also lost and, in addition, the company must also bear the cost of expensive spare parts. In the market, demand is uncertainty and if the productivity is much greater than demand, excess product will accumulate in the warehouse and inventory cost will be high. Therefore, there is a need to develop aggregate production model for businesses that can solve these unplanned outage issues, and customer requests can also be met successfully. A cost analysis was carried out for the proposed model and detailed discussions and recommendations were made.

2. LITERATURE REVIEW

To be effective, aggregate planning requires input from all stages of the supply chain, and the results have an extraordinary impact on supply chain performance. Collaborative forecasts are made by many companies in the supply chain and are important inputs for aggregate planning (Sunil Chopra, 2016). In addition, many of the obstacles that constitute the main input for aggregate planning come from supply chain partners outside the company. Without this input, both from above and below the supply chain, aggregate planning cannot realize its full potential to create value. The results of aggregate planning are also valuable for upstream and downstream partners. The production plans for the company determines supplier demand and establishes supply limits for customers. Nam and Logendran (1992) defined aggregate production planning, including access to the organization's production, storage capacity and workforce in a limited period of time. The objective of the aggregate production planning is to maximize the utilization of the company's resources and benefits, deliver on time to customers, and minimize overall

costs and inventory. Subrata Talapatra, et al. (2015) proposed an aggregate planning model based on linear programing. That paper mainly focuses on experimenting with workforce. Ghulam Asghar, et al. (2015) studied an alternative model of aggregate production planning for the process industry. This investigation was conducted in accordance with six-month demand forecasts from Pakistan's leading cement industry. Various alternatives have been discussed and the proposed model has been developed and analyzed. Mohamed K. Omar, et al. (2013) has developed a Fuzzy Mixed Integer Linear Programming Modeling (FMILP) approach to address multi-product application problems faced by special chemical plants. The aim of the proposed model is to minimize the amount of production, configuration, inventory, pending orders and labor costs. The model formulation combines fuzzy set theory and probability theory to determine the uncertainties that arise in the aims and limitations of the model. Anand Jayakumar, et al. (2017) studied aggregate planning problem using Lingo software. The goal of this paper is to minimize profit while meeting demand. This paper used Lingo software to solve numerical problem. Navid Mortezaei, et al. (2013), developed a new multi-purpose linear programming model for general aggregate production planning for multiple period multi product problems. This model assumes that there is uncertainty in the input of critical data. This model is suitable for a 24-hour production system. To demonstrate the practicality of the model, the model was implemented as a case study. In this study also will be developed a liner-programming model to solve the aggregate production planning of a cement industry.

3. RESEARCH METHODOLOGY

Methodology is considered step-by-step procedure for the implementation of aggregate production plan. This research will be implemented an aggregate production planning of a cement industry as shown in figure 1. In this study, at first the needed data were collected to develop linear programming model as shown in table 1 and table 2. After collecting the data, linear programming model was developed and formulated the objective function and constraint equations of the model. And then Lingo software was used to solve the model. After solving the model, obtained solutions are evaluated and if the solutions are not satisfied, the model is developed again to get the feasible solution. If the solutions are satisfied, aggregate production plan will be implemented.

Table 1. Demand forecast for six months

No	Months	Demand (tons)
1	July	28600
2	August	25000
3	September	27000
4	October	30280
5	November	29065
6	December	32300

Table 2. The data related to production cost

Operation cost	Ks32400000/day
Raw materials cost	Ks27000/ton
Inventory cost	Ks3000/ton/month
Shortage cost	Ks12000/ton
Subcontracting cost	Ks63000/ton
Production capacity	36000 ton/month
Maximum working day	25 day/month
Opening inventory	3600 tons
Ending inventory	3600 tons

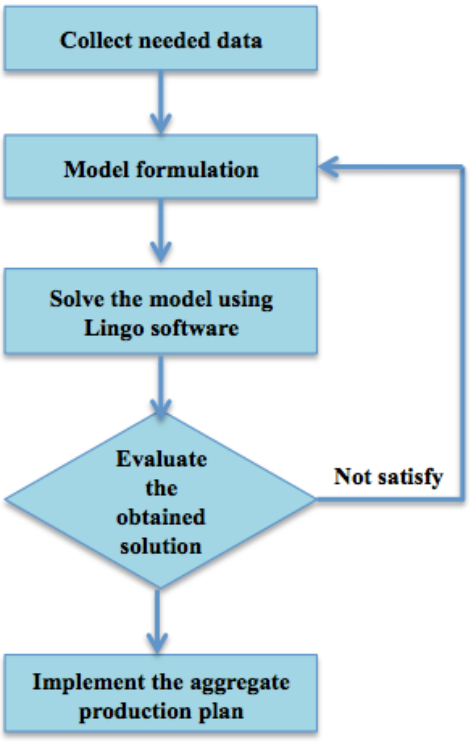

Figure 1. Research Methodology flow chart

4. MODEL DEVELOPMENT

In order to solve optimization problem, an aggregate production-planning model is implemented. To find the best possible solution, Linear Programming (LP) model is used to optimize the aggregate production plan of a cement industry. The following mathematical formulations are used to develop (LP) model.

2) 4.1. Indices and Sets

t = index for time periods (month); t ϵ T

3) 4.2 Model Parameters

OD = Operating cost per day of the industry (Ks/day)
RT = Raw materials cost (Ks/ton)
IT = Inventory cost (Ks/ton/month)
ST = Shortage cost (Ks/ton/month)
CT = Subcontracting cost (Ks/ton/month)
PR = Production rate (ton/day)
MA = Allowable operating days (day/month)

4) 4.3 Decision Variables

W_t = Number of operating days in month (t) (day/month)

P_t =Production plan in month (t)(ton/month)

I_t =Amount of inventory in month (t) (ton/month)

S_t =Amount of shortage in month (t) (ton/month)

B_t =Amount of cement bought from subcontractor in month (t) (ton/month)

5) 4.4 Objective function

Minimize Cost

$$\sum_{t\in T}(OD * W_t) + \sum_{t\in T}(RT * P_t) + \sum_{t\in T}(IT * I_t) + \sum_{t\in T}(ST * S_t) + \sum_{t\in T}(CT * B_t) \quad (1)$$

The objective function of the model is to minimize the cost for six month, including total operation cost, total raw material cost, total inventory cost, total shortage cost and total cost of subcontracting.

6) 4.5 Constraints

$$P_t \leq PR*W_t \qquad \forall t \in T \qquad (2)$$

The amount produced in the plants for all period cannot exceed its capacities.

$$W_t \leq MA \qquad \forall t \in T \qquad (3)$$

The number of operating days in all periods is less than maximum allowable operating days from factory management.

$$I_{t-1} + P_t + B_t = D_t + S_{t-1} + I_t - S_t \qquad \forall t \in T \quad (4)$$

The sum of opening inventory, productivity in month (t) and quantity brought from subcontractor in month (t) equal to the sum of demand in month (t), the amount of shortage from previous month and ending inventory in month (t) subtract the amount of shortage in month (t).

$$W_t \geq 0 \qquad \forall t \in T \qquad (5)$$

The number of operating days in month (t) must be greater than or equal to zero.

$$I_t \geq 0 \qquad \forall t \in T \qquad (6)$$

The amount of inventory in month (t) must be greater than or equal to zero.

$$S_t \geq 0 \qquad \forall t \in T \qquad (7)$$

The amount of shortage in month (t) must be greater than or equal to zero.

$$B_t \geq 0 \qquad \forall t \in T \qquad (8)$$

The amount of product bought from subcontractor in month (t) must be greater than or equal to zero.

5. LINGO PROGRAM

```
Model:
Min = Totalcost;
Totalcost = OC+RC+IC+SC+CC;
OC = OD*(W1+W2+W3+W4+W5+W6);
RC = RT*(P1+P2+P3+P4+P5+P6);
IC = IT*(I1+I2+I3+I4+I5+I6);
SC = ST*(S1+S2+S3+S4+S5+S6);
CC = CT*(B1+B2+B3+B4+B5+B6);
P1 <= PR*W1; P2 <= PR*W2; P3 <= PR*W3;
P4 <= PR*W4; P5 <= PR*W5; P6 <= PR*W6;
W1 <= MA; W2 <= MA; W3 <= MA;
W4 <= MA; W5 <= MA; W6 <= MA;
OD = 32400000; RT = 27000; IT = 3000;
ST = 12000; CT = 63000; PR = 1200;
MA = 25; I0 = 3600; S0 = 0; I6 = 3600; S6 = 0;
D1 = 28600; D2 = 25000; D3 = 27000;
D4 = 30280; D5 = 29065; D6 = 32300;
I0 + P1 + B1 = D1 + S0 + I1 - S1;
I1 + P2 + B2 = D2 + S1 + I2 - S2;
I2 + P3 + B3 = D3 + S2 + I3 - S3;
I3 + P4 + B4 = D4 + S3 + I4 - S4;
I4 + P5 + B5 = D5 + S4 + I5 - S5;
I5 + P6 + B6 = D6 + S5 + I6 - S6;
W1 >= 0; W2 >= 0; W3 >= 0;
W4 >= 0; W5 >= 0; W6 >= 0;
I1 >= 0; I2 >= 0; I3 >= 0;
I4 >= 0; I5 >= 0; I6 >= 0;
S1 >= 0; S2 >= 0; S3 >= 0;
S4 >= 0; S5 >= 0; S6 >= 0;
P1 >= 0; P2 >= 0; P3 >= 0;
P4 >= 0; P5 >= 0; P6 >= 0;
B1 >= 0; B2 >= 0; B3 >= 0;
B4 >= 0; B5 >= 0; B6 >= 0;
@GIN(W1); @GIN(W2); @GIN(W3);
@GIN(W4); @GIN(W5); @GIN(W6);
@GIN(I1); @GIN(I2); @GIN(I3);
@GIN(I4); @GIN(I5); @GIN(I6);
@GIN(S1); @GIN(S2); @GIN(S3);
@GIN(S4); @GIN(S5); @GIN(S6);
@GIN(P1); @GIN(P2); @GIN(P3);
@GIN(P4); @GIN(P5); @GIN(P6);
@GIN(B1); @GIN(B2); @GIN(B3);
@GIN(B4); @GIN(B5); @GIN(B6);
End
```

6. RESULTS AND DISCUSSION

By optimizing the objective function subjected to the constraints the simulation results of aggregate production plan is shown in the figure 2. The detail proposed aggregate production plan is shown in table 3 and table 4. Total cost of the proposed aggregate production plan for the six months planning horizon is Ks 9362.16 million. The current estimate cost of the company for the six month production plan is Ks 9883.125 million. The company uses level production strategy for the current production and factory has to produce 25 days in every moth. The production cost of the current plan is greater than the proposed plan. So, the proposed aggregate production plan can save Ks 520.965 million and this amount will contribute to company's profit directly. According to the company policy, the beginning inventory and ending inventory are set by 3600 tons. This amount is equal to the three days production of the industry because factory production rate is 1200 ton per day. The number of operating days in July and August are 21 days and September is 23 days and October, November and December are 25 days because the demand is high in these three months. Factory uses the subcontractor during the month of December. In all months, there is no shortage. In fact factory carries inventory in all periods. But, the amount of carrying inventory is not much and it is carried in anticipation of a future increase in demand.

Table 3. Results of Inventory, shortage and subcontract

Months	Inventory (tons)	Shortage (tons)	Subcontract (tons)
July	200	0	0
August	400	0	0
September	1000	0	0
October	720	0	0
November	1655	0	0
December	3600	0	4245

Table 4. Results of operating days and production plan

Months	Operating days	Production plan (tons)
July	21	25200
August	21	25200
September	23	27600
October	25	30000
November	25	30000
December	25	30000

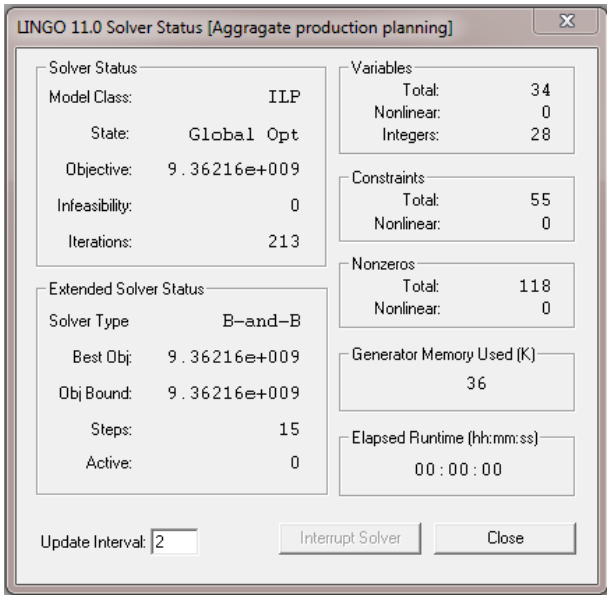

Figure 2. Simulation results of lingo program

7. CONCLUSION

From the above results and discussion it has been identified the aggregate production planning model of the cement plant. The proposed model determines the better production and inventory plan to minimize the overall cost. By developing the model there is no need to carry excess inventory and the inventory holding cost will be low. There is no shortage in all periods. Thus customer service level will be high. Therefore the aggregate production-planning model is better suited for the selected cement plant as well as for other cements industries.

ACKNOWLEDGEMENT

The author would like to express his gratitude to Dr. Myint Thein, Rector of the Yangon Technological University, for giving permission to submit this paper in journal. The author wishes to express his gratitude to Dr. Mi Sandar Mon, Professor and Head of the Department of Mechanical Engineering of the Yangon Technological University for her permission and encouragement to write this paper. The author would like to thank to his supervisor Dr. Yin Yin Tun, Professor of the Department of the Mechanical Engineering of the Yangon Technological University, for her encouragement, kind suggestion and sharing her knowledge.

REFERENCES

[1] Sunil Chopra and Peter Meindl, Supply Chain Management: Strategy, Planning and Operation, sixth edition, 2016.

[2] S. j. Nam and R. Logendran, "Aggregate production planning—a survey of models and methodologies," European Journal of Operational Research, vol. 61, pp. 255-272, 1992.

[3] Subrata Talapatra, Moumita Saha, Md. Abnul Islam, Aggregate planning problem solving using linear programming method, American Academic & Scholarly Research Journal Vol. 7, No. 1, Jan 2015.

[4] Ghulam Asghar, Wasif Safeen, Mirza Jahanzaib, An alternate model of aggregate production planning for process industry: a case of cement plant, Technical Journal, Vol. 20(SI) No II (S) , 2015, pp 12 – 18.

[5] Mohamed K. Omar, Muzalna Mohd Jusoh and Mohd Omar, Fmilp formulation for aggregate production planning, World Applied Sciences Journal 21 (Mathematical Applications in Engineering): pp 68-72, 2013.

[6] Anand Jayakumar AP P, Krishnaraj CP P and Balakrishnan S, Solving Aggregate Planning Problem Using Lingo, IJISET - International Journal of Innovative Science, Engineering & Technology, Vol. 4 Issue 12, December 2017 ISSN (Online) 2348 – 7968 | Impact Factor (2016) – 5.264.

[7] Navid Mortezaei, Norzima Zulkifli, Tang Sai Hong, Rosnah Mohd Yusuff,, ―Multi-objective aggregate production planning model with fuzzy parameters and its solving methods‖, Life Science Journal 2013;10(4), pp. 2406 – 2414.

NUMERICAL SIMULATION OF ROTOR-STATOR IN PROPELLER TURBINE

Khin Ohnmar Myo[(1)], Aye Thwai Thwai Tun[(2)], Cho Cho Khaing[(3)]
[(1)]Department of Mechanical Engineering, Technological University (Sittwe)
[(2)] Department of Mechanical Engineering, Hakha College
[(3)]Faculty of Precision Engineering, University of Technology (Yatanarpon Cyber City)

Email: chokhaing1@gmail.com

ABSTRACT: The purpose of this paper describes the numerical simulation of rotor-stator in propeller turbine. In this paper, the design of 30 kW propeller turbine is expressed. The available head and flow rate are 9 m and 0.56 m^3/s respectively. These data are taken from Upper Paunglaung Dam. Propeller turbines are well suited for these types of applications. This paper focuses on flow phenomena such as potential interaction and dynamic load on runner blades and guide vanes are analyzed. Moreover, the resistance of blade stresses and strains are simulated on the various pressures and forces by CFD software package. A numerical study of the water velocity conditions in rotor and stator has been conducted for a wide range of passage widths with the commercial Computational Fluid Dynamics (CFD) code Fluent 6.1.22. CFD validation has been performed.

Keywords— *dynamic load, pressure distribution, propeller turbine, smaller head, unsteady rotor –stator interaction, velocity distribution.*

1. INTRODUCTION

One of the most useful natural energy sources to fulfill the electricity requirement is hydro-electric power project. Therefore, natural source of water can provide that required power for farms, schools, hospitals and rural communities.

Propeller Turbine is reaction type turbine. This turbine convert the water energy into mechanical energy. The water energy may be either in the form of potential energy such as dams, reservoirs, or in the form of kinetic energy in flowing water. The shaft of the turbine directly coupled to the electrical generator which converts mechanical energy into electrical energy. This is know as hydro-electric power. This turbine has adjustable blades. It was developed in 1913 by Austrian professor viktor, who combined automatically adjusted propeller blades with automatically adjusted wicket gates to achieve efficiency over a wide range of flow and head. Gagnon J.M, Deschenes C, [3] describes increasing the number of blade the force acting on the blade reduces. But material cost increases with increasing number of blades.

In this paper describe the design and numerical simulation with the design condition. Moreover, it is required to avoid the damages due to the unsteady effect in rotor and stator while operating. This paper will discuss the about the unsteady interaction in rotor and stator of propeller turbine [2].

1.1. Reaction turbine

The reaction turbines considered here are the Francis turbine, bulb turbine, tubular turbine and the propeller turbine. A special case of the propeller turbine is the Kaplan. In all these cases, specific speed are high, i.e reaction turbines rotate faster than impulse turbines given the same head and flow conditions [2].

1.2. Propeller Turbine

Propeller turbine is axial flow reaction turbine, generally used for low head.

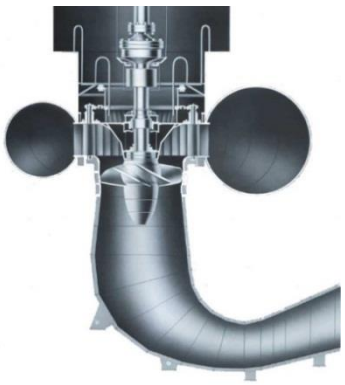

Fig. 1 Runner of Propeller Turbine [3]

The basic propeller turbine consists of a propeller, similar to a ship's propeller, fitted inside a continuation of the penstock tube. The propeller usually has three to six blades, three in the case of very low head units and the water flow is regulated by static blades or swivel gates just upstream of the propeller. This kind of propeller turbine is known as a fixed blade axial flow turbine as shown in Fig. 1. The pitch angle of the rotor blades cannot be changed.

2. BASIC COMPONENT OF PROPELLER TURBINE

The components of a propeller turbine are:

(1) Spiral casing
(2) Runner
(3) Guide Vanes
(4) Draft tube

2.1. Spial Casing

The Francis and propeller types require a flume or case, the main function of which is to distribute the water as uniform and smoothly as possible around the circumference of the guide case in order to obtain maximum power and efficiency [6].

2.2. Guide Vane

The purpose of the guide blade is to supply the water to the runner at a certain velocity and in a certain direction in such a way that these values are the same for the entire circumference. It follows from the discharge part of the guide blade is of importance, whilst from its other part only the prevention of superfluous losses is required. For this reason it is not necessary in turbines of different sizes to have the same number of blades as in the model [6].

2.3. Runner

Runner is the main component of the turbine that converts water power to the rotation of shaft power. The velocity of water from spiral casing which passes through the guide vanes then passes through a curved shape series of runner. So the relative velocity of the water is always tangent to the vane.

3. BASIC THEORIES OF PROPELLER TURBINE

The basic theories of propeller and Kaplan turbine are the same as well as in following.

3.1. Specific Speed and Head Limitation

The specific speed is a type of characteristic where all runners of a given specific speed are similar in form and vary only in size. This speed forms a basis for classification of turbines.

$$N = \frac{N_s \sqrt{P_t}}{H_d^{1.25}} \quad (1)$$

where

N_s = Specific speed (rpm)
N = Unit speed (rpm)
H_d = Design head (m)
P_t = power output of the turbine (kW)

Calculating the specific speed of the turbine after knowing the design net head (H_d). The specific speed can be calculated from the following equation. For head less than 18m – fixed blade propeller turbine [5],

$$N_s = \frac{885.5}{H_d^{0.25}} \quad 2$$

Turbines with low specific speeds work under high head and low discharge conditions, while high specific speed turbines work under low head and high discharge conditions.

Table 1. Relationship between head and turbine type

Type of Turbine	Limit of Head	Specific Speed
Pelton turbine	300 to 2000 m	4 to 70
Cross flow	10 to 100 m	40 to 200
Francis	60 to 400	
Kaplan, Propeller	2.5 to 450 m	300 to 1100
Fixed blade Propeller	1.5 to 70 m 1.5 to 30 m	300 1000

3.2. Workdone and Efficiency of the Turbine

The expression for the power delivered to the shaft by passing water is the same for all types of reaction turbines. In this case, it is necessary to use velocity diagram and Euler's Equation to calculate the power and efficiency of the turbine. Inlet and outlet velocity triangle of propeller turbine is indicated in Fig. 2.

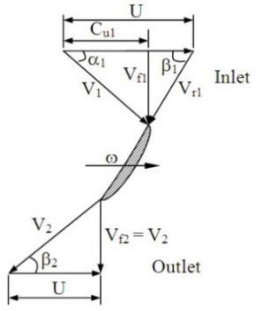

Fig. 2 Schematic Diagram of Automatic Transmission [5]

where

U = runner tangential velocity (m/s)
ω = runner angular velocity (m/s)
V = fluid absolute velocity (m/s)
V_r = fluid relative velocity (m/s)
C_{u1} = fluid whirl velocity (m/s)
β = runner blade angle (deg)
α = guide vane angle (deg)

The runner tangential velocity,

$$U = \frac{\pi D n}{60} \quad (3)$$

The runner angular velocity,

$$\omega = \frac{2U}{D} \quad (4)$$

The hydraulic efficiency,

$$\eta_h = \frac{(C_{u1}U_1 - C_{u2}U_2)}{g\,H}$$

(5)

where,

g = acceleration due to gravity (m/s)
H = design head (m)

3.3. Runner Blade

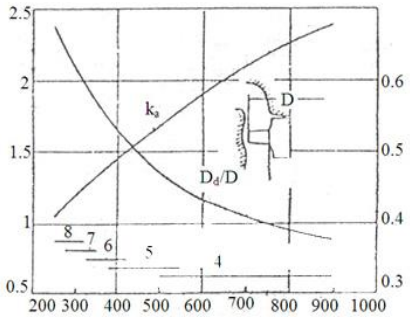

Fig. 3 Relationship between Speed Ratio and Specific Speed [1]

The outer diameter of the runner [1],

$$D = \frac{84.5 \times \phi \times \sqrt{H_d}}{N} \quad (6)$$

$$\phi = 0.0242 \times N_s^{2/3} \quad (7)$$

where

H_d = design head (m)
N = runner speed (rpm)
N_s = specific speed (rpm)

The inner diameter, d can be obtained by using the Fig.3 depending on the specific speed, N_s.

3.4. Runner Blade Angle

The runner blade angle is between the tangential velocity of runner and the relative velocity of water. It can be define by the following equations [5].

Inlet blade angle,

$$\tan\beta_1 = \frac{V_{f1}}{U - V_{w1}} \quad (8)$$

Outlet blade angle,

$$\tan\beta_2 = \frac{V_{f2}}{U - V_{w2}} \quad (9)$$

3.5. Guide Vane Angle

The main important is the correct design of the outlet blade angle, which must correspond to the velocity diagram. The angle of the outlet part in the one dimensional solution is given by the velocity at the outlet edge of the guide blade. The outlet blade angle of guide vane can be calculated [7].

$$\tan\alpha = \frac{V_f}{C_{u1}} \quad (10)$$

where

V_f = Flow velocity (m/s)
C_{u1} = Component of absolute velocity (m/s)

3.6. Circulation

The water approaches the blade at the velocity C_1 which incorporate a certain peripheral component C_{u1}. That is in the form of a whirl with its axis in the turbine axis and the circulation can define as follow [7];

$$\Gamma_1 = 2\,\pi\,r\,C_{u1} \quad (11)$$

where

Γ = circulation (m^2/s)
t = spacing of the blade (m)

C_u = tangential component of absolute velocity (m/s)

The spacing of the blade

$$t = \frac{2\pi\ r}{z} \quad (12)$$

3.7. Power and Flow Rate at Variable Head

Knowing the efficiency, speed, power and discharge of a runner of a given diameter at a given head, calculated directly the following equations for the same efficiency [7].

For constant diameter,

$$\frac{P_2}{P_1} = \left(\frac{H_2}{H_1}\right)^{3/2} \quad (13)$$

$$\frac{Q_2}{Q_1} = \left(\frac{H_2}{H_1}\right)^{1/2} \quad (14)$$

4. DESIGN OF 30KW PROPELLER TURBINE

In design consideration of a turbine from Upper Paunglaung, the hydraulic efficiency, the best speed for maximum efficiency and synchronous speed are necessary in design calculation. In this paper, overall efficiency and mechanical efficiency are assumed such as 68 % and 85 %.

To obtain 30 kW for four pole generator, the turbine speed to drive the generator must be about 1500 rpm. The design head is 9 m and design calculations are as followed.

The required generator output power, P_g = 30 kW
Generator efficiency, η_g = 0.8
Generator speed, N_g =1500 rpm
Design head of turbine, H_d = 9 m
Mechanical efficiency, η_m = 0.85

The results data of the propeller turbine is as shown in Table 2.

Table 2. Results data of 9m head for 50kW

Item	Result Data
Turbine power, P	44.12 kW
Turbine speed, N	1199 rpm
Flow rate, Q	0.56 m^3/s
Runner outer diameter, D	327 mm
Hub diameter, d	154 mm
Height of the hub or boss	356.7mm
Length of guide vane, L	111mm
Height of guide vane, B	130.8 mm
Number of guide vane, N_g	10
Number of runner, z	4

4.1. Variable Head in Propeller Turbine

If the turbine is working under different head, the power and flow rate of the turbine can be easily known from the following Table 3.

Table 3. Power and flow rate at variable head

Head (m)	**Power (kW)**	**Flow Rate(m^3/s)**	**Efficiency (%)**
6	24.02	0.457	89
8	36.97	0.528	89
10	51.67	0.590	89
12	37.93	0.647	89
14	85.59	0.698	89

4.2. Runner Blade Dimensions

The runner dimensions of the section –I, II, IV, V and IV are discussed in the Table 3.2 shown below.

Table 4. Results data of blade profile

Item	I	II	III	IV	V
$r_1 = r_2$(m)	0.0792	0.1004	0.1216	0.1401	0.1586
$U_1 = U_2$(m/s)	9.94	12.61	15.27	17.59	19.91
V_f (m/s)	8.62	8.62	8.62	8.62	8.62
v_{w1} (m/s)	7.91	6.23	5.15	4.47	3.95
α_1 (deg)	47.46°	54.14°	59.14°	62.59°	65.38°
β_1 (deg)	76.75°	53.49°	40.42°	33.31°	28.37°

β_2 (deg)	40.93°	34.36°	29.44°	26.11°	23.41°
t (m)	0.1244	0.1577	0.191	0.2201	0.2491
Γ (m^2/s)	0.984	0.9825	0.9837	0.9838	0.9839

4.2Design of Shaft

Specification data of shaft design is as follow,
Shaft material = 40C8 Carbon Steel
Allowable shear stress, s_{sall} = 96 MPa
Generator power, P_g = 30 kW
Shaft speed, N_s =1199 rpm
Turbine tangential force, F_t = 2199.42 N
Turbine axial force, F_a = 3637.4N
Shaft length, L_1 = 200 mm
Shaft length, L_2 = 230 mm
Runner mean radius, r_m = 120 mm
Moment factor, k_b = 3
Torque factor, k_t = 3

The shaft of propeller turbine is solid and the axial load is applied. So, the applied stress on the shaft is defined as,

$$s_s = \frac{16}{\pi d_s^{\,3}} \sqrt{\left[k_b M_b + \frac{\alpha F_a d_s}{8}\right]^2 + (k_t M_t)^2}$$

(15)

where
d = shaft diameter, m
α = axial load factor
N = the speed of turbine, rpm
M_b = bending moment, N m
M_t = torsional moment, N m

The shaft diameter of 50 mm is satisfied because the actual applied stress, s_s is 62.949 MPa. Therefore, it is less than the allowable shear stress, s_{sall} of 96 MPa. The selected diameter is satisfied for design.

5. NUMERICAL SIMULATION

In this section, the designed data which are calculated in designed section will be checked the velocities and pressures through the guide vane and the runner by using FLUENT 6.1.22 software. It is need detailing drawing. So, in this paper, the Auto CAD software is used to draw detail drawing. The flow of software implementation is as shown below. The data are taken from the design section and other processes of this section are as shown below.

5.1. Computational Domain

Boundary conditions are defined as periodic on both side of the rotor and stator domains. Inlet condition at the stator domain is constant flow oriented in a standard direction for a semi-spiral casing. Runner outlet condition is fixed with constant relative static pressure.

Table 5. Parameter

Parameters	Value	unit
Re_D	$2.3e^6$	-
Re_L	$1.5e^6$	-
Viscosity	0.001003	kg/m.s
Rotational speed	1500	rpm
Required shaft power	44.12	kW
Max efficiency	85	%

Re_D based on rotor diameter.
Re_L based on guide vane chord length.

The governing equation is

$$A_s\left(\frac{-dH}{dt}\right) = C_d A_o \sqrt{2gH}$$

In this paper, the 2D drawing is required to run the results. The results drawing of the design are as shown in Fig. 4.

TABLE I
Result data of n.a.c.a- 4412 blade profile dimensions

Parameters	I	II	III	IV	V
$R_1 = R_2$(m)	0.0657	0.0934	0.1212	0.1347	0.1481
$U_1 = U_2$(m/s)	6.7396	9.5881	12.4364	13.8196	15.2027
V_f(m/s)	6.7654	6.7654	6.7654	6.7654	6.7654
β_1(degree)	77°	48.69°	35.09°	30.93°	27.66°
β_2 (degree)	45.11°	35.21°	28.55°	26.08°	23.99°
C_{u1} (m/s)	5.18184	3.6424	2.8082	2.5271	2.2972
$W_{\alpha 1}$ (m/s)	4.14868	7.6669	11.0323	12.5561	14.0541
β_α (degree)	58.48°	41.06°	31.52°	28.32°	25.71°
W_α (m/s)	7.93615	10.3006	12.9418	14.2632	15.5983
t (m)	0.09	0.051	0.066	0.074	0.081
Γ (m^2/s)	0.4664	0.4664	0.4664	0.4664	0.4664
l/t	1.1000	1.0125	0.925	0.84	0.74
l= l/t × t (m)	0.099	0.129	0.155	0.16	0.157
β (degree)	41.52°	58.94°	68.48°	71.68°	74.29°
α (degree)	10°	6°	3.5°	2.7°	1.5°

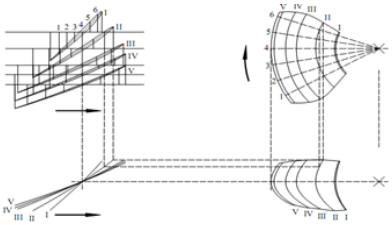

Fig. 4 All section view of blade

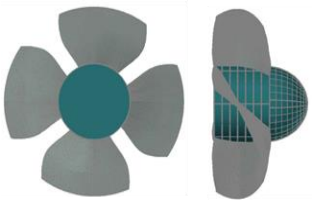

Fig. 5. Top view and side view of runner

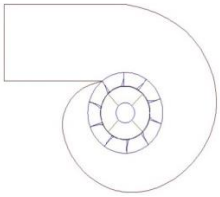

Fig. 6. 2D Drawing of Runner and Casing with Design Specification

5.2. CFD SIMULATION

The calculated design of blade is simulated on the various pressures by CFD software. Before simulating, design of the blade profile is drawn with AutoCAD software. And then, mesh generation is made by using SolidWork software. After that, these designed drawings are exported into the Ansys CFD software.

After running 2000 numbers of iteratrions, satisfied converged solutions is obtained.

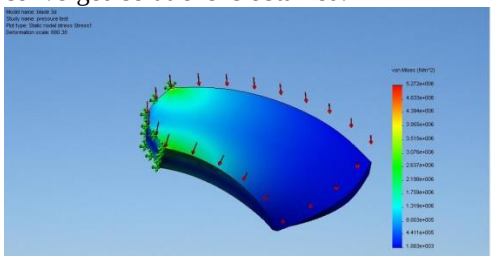

Fig. 7. CFD application of pressure test on stress analysis

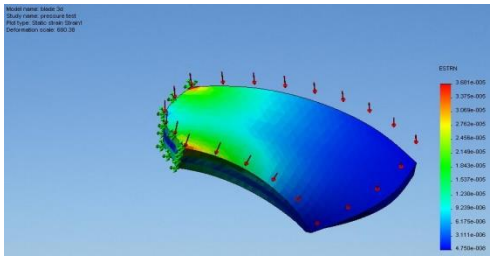

Fig. 8. CFD application of pressure test on strain analysis

5.2. FLUENT Results

The FLUENT result of velocity diagram is as well as in Fig. 9.

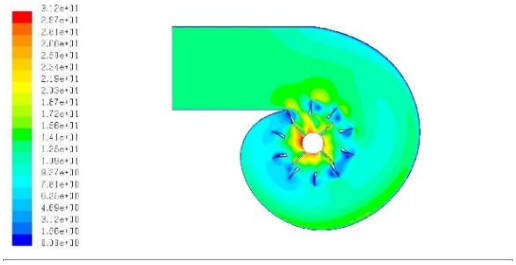

Fig. 9 Contours of Outlet Velocity

The FLUENT result of static pressure diagram is as well as in Fig. 10.

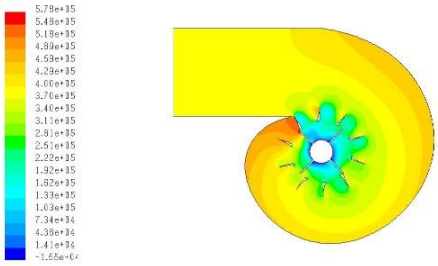

Fig. 10 Contours of Static Pressure

The FLUENT result of dynamic pressure diagram is as well as in Fig. 11.

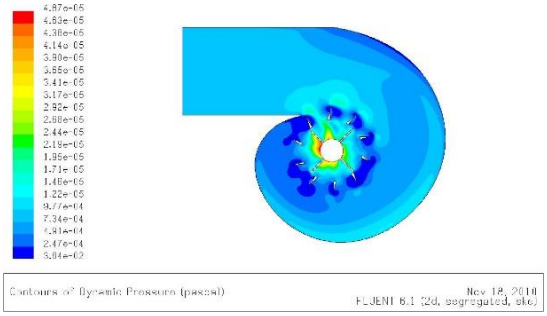

Fig.11. Contours of Dynamic Pressure

The FLUENT result of total pressure diagram is as well as in Fig. 12.

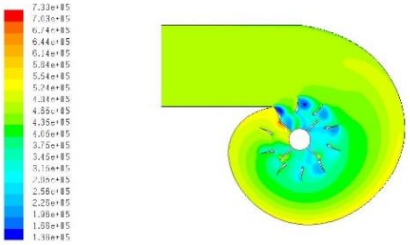

Fig. 12. Contours of Total Pressure

6. CONCLUSION

The velocity distribution of the area among guide vanes and runners calculated by FLUENT 6.1.22. The velocity values back of the vane is lowest and the values are about zero. The solution is converge (stable) after around 400 calculation (iterations). The net mass flow rate checked also FLUENT 6.1.22 software. The net mass flow rate is 10^{-2} kg/s.

In this paper, the propeller turbine is designed for 9 m head and 0.56 m^3/s flow rate to generate 30kW power. The calculated runner diameter is 250 mm, hub diameter is 95 mm and number of blade is four. The runner blade is divided into five cylindrical sections. The available head distributions are calculated by using MATLAB programming and the detail drawing is drawn by AutoCAD software. Finally, ANSYS software is used to test the structure of the blade of the turbine. The pressures act on the blade from 15,000 Pa to 50,000 Pa. The forces which are normal act from 150 N to 500 N. The unsteady interaction between the rotors and stators is check with FLUENT 6.1.22 software. The inlet velocity is weak behind the stator and high at inlet of the rotor and the outlet velocity is the highest at the stator outlet. The static pressure is high in the stator inlet and weak at the rotor outlet. The dynamic pressure is weak behind the stator and high at the rotor base. The design calculation of 30 kW propeller turbine and three dimensional runner blade profile has been described in this paper. This turbine design is reasonable with actual design from Upper Paunglaung.

REFERENCES

[1] Celso. P and Dr. Ingeniero. D.M, Layman's Handbook on How to Develop a Small Hydro site, European Small Hydropower Association, (1998).

[2] Dermot McGuigan, Harnessing Water for Home Energy, (1944).

[3] Gagnon J.M, Deschenes C, Numerical Simulation of a Rotor-Stator Unsteady Interaction in a Porpeller Turbine, (2010).
[4] Kumar, D.S, Fluid Mechanics and Fluid Power Engineering, Punjab Engineering College, 6th Edition, (1998).
[5] Miroslav. N, Hydraulic Turbine their Design and Equipment, ARTIA Prague, Czechoslovakia, (1957).
[6] Nyein Wai, Design Modification of Blade Profile for Low Head Propeller Turbine, Ph.D Paper, (2009).
[7] S. Cody Maher, Microhydro Turbine (FUS Micro Hydro Project), September, (2006).
[8] TOSHIBA Power System and Service Company, Catalog of Hydraulic Turbine, Tokyo, Japan, (2010).

Replacing Spur Gear with Helical Gear in Power Transmission System for Upland Tiller

1 Dr Aung Zaw Tun, 2 U Phyo Wai Linn, 3U Ko Ko
1 Technological University (banmaw), Banmaw, Myanmar
2 Technological University (panglong), Shan, Myanmar
3 Technological University (kalay), Sagaing, Myanmar

aungzawtun.eng@gmail.com

ABSTRACT: The aim of this paper is to use helical gears in place of spur gears for power transmission for Upland Tiller. The helical gear is smoother to drive than the spur gear, making the driver more comfortable in the field. In the design of manual transmission gearbox, main components of gearbox housing, shafts and gear can be obtained locally. Farmers use 7.46 kW engine of Upland Tiller at field operation. Analytical results are based on Lewis formula. The original power transmission system uses gear and pinion for the spur gear type. Helical gears operate more smoothly and silently when compared to spur gears. This difference is due to the oblique manner in which their teeth interact in relation to the rotational axis. This axis may be parallel or generally crossed at 90°. In case it is crossed, helical gears are applied together with a worm gear, even though on these cases, two bevel gears may alternatively be used. When two of the teeth move, contact is gradual, beginning at one end of the tooth, and staying in contact with the gear, which rotates until full contact is achieved. On the other hand, the thrust load varies in direct proportion to the magnitude of the tangent of the helix angle [1].In this paper, in order to make some modifications; the design of the helical gear is calculated by using new materials without changing the velocity ratio, center distance and original housing design. Different material can also be tried for weight and cost optimization. To calculate reliable strength and dynamic load of the gear lewis equation is employed.

KEYWORDS: Upland Tiller, Transmission gearbox, Spur gear, Helical gear.

1. INTRODUCTION

Power tillers or two wheels tractors are used for tilling of seedbed in small farms and in hill farming and for carrying out spraying operations in horticultural crops and food crops. The adaption of power tillers by the farmers for carrying out farming operations is low when compared to tractors. Upland tiller has power rating (7.46 kW) at 2200 rpm. The gearbox is selective sidling mesh type which is designed to transmit the power from engine to the final drive. Upland tiller has two types of control system. They are walking type and riding type. Power tiller is a walking type tractor. The operator trails behind the power tiller, holding the two handles of tiller in his hands. Now–a–days some model of power tillers have been especially designed and developed for use on small or medium farms where four wheel tractors are not easily available[2].

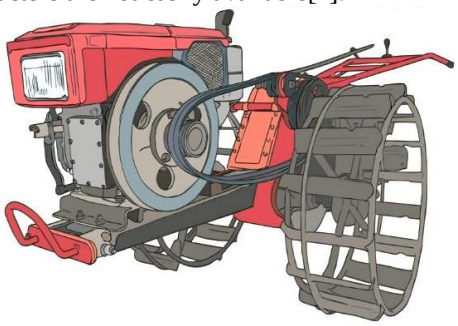

Figure1. Upland Tiller.

There are four speed in power transmission syetem (first, second, third and reverse).In this paper, second speed position is analised.

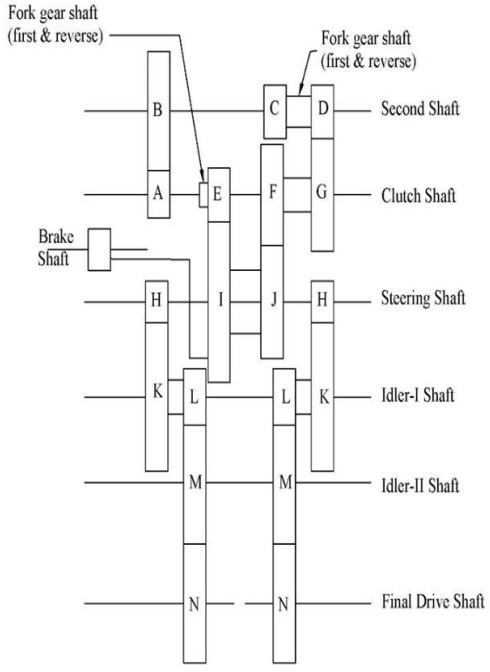

Figure 2. Upland tiller gear box arrangement (second speed)

2. TYPES OF GEARS

2.1 Spur Gear

Spur gears have their teeth parallel to the axis and are used for transmitting power between two parallel shafts. They are simple in construction, easy to manufacture

and cost less. They have the highest efficiency and excellent precision rating. They are used in high speed and high load application in all types of trains and a wide range of velocity ratios. Hence, they find wide application from clocks household gadgets, motor cycles, automobiles, and always to aircrafts. Figure 3. shows the spur gear[3].

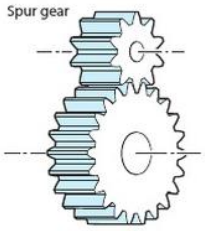

Figure 3. Spur gears

2.2 Helical Gear

Helical gears are used for parallel shaft drives. They have teeth inclined to the axis as shown in Figure 4. Hence for the same width, their teeth are longer than spur gears and have higher load carrying capacity. Their contact ratio is higher than spur gears and they operate smoother and quieter than spur gear. The precision rating is good.

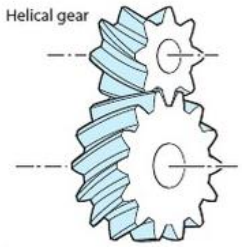

Figure 4. Helical gears

2.3 Advantages of Helical Gears

The angled teeth work more gradually, allowing for smoother and more silent gear operation when compared to spur gears or toothed wheels.

(1) Helical gears last longer and are ideal for high-load applications, since they have a higher amount of teeth in contact.

(2) Load is at all times distributed among several axes, which produces less wear.

(3) They can transfer motion and power both among parallel and straight-angle axes.

3. SELECTING GEAR MATERIAL

When load to flank of gear is excessive, wearing off (pitting) of flank may occur easily. It is necessary to select material with greater strength of surface durability therefore the case hardening steel is recommended due to higher hardness.

The impact to flank of gear during operations causes damage to the gear tooth; therefore it is necessary to select steel with higher bending strength. Selected material should be able to apply induction hardening after quenching and annealing treatment. Such selection emphasizes on core hardness instead of surface strength. The following facts should be considered, while selecting of material in manufacturing.

(1) For necessary strength for gear, select the material character by emphasizing on either Surface durability or Bending strength. Generally, ideal material selected for gear tooth should be tough and hard to withstand damaged by the load.

(2) Suitable material for machining. Pitting occur easily in free cutting steel even after surface treatment is applied to gear. This material is unsuitable for gear even though it has good machinability.

(3) Material could be easy to apply heat treatment and little deformation. Even if deformed after applying heat treatment, amount should be stable.

(4) Material should be economical and easily obtained.

4. DESIGN CONSIDERATION FOR GEAR DRIVE

4.1 For Spur Gear

The pitch line velocity is derived from the basic relationship, for

$$V = \frac{\pi D_p (rpm)_p}{60} \qquad (1)$$

where, Dp = pinion diameter, m

rpm = rotational speed of the pinion, rpm

The transmitted force can be found by dividing the power transmitted by the pitch line speed.

$$M_t = \frac{9550 \times kw}{rpm} \qquad (2)$$

Transmitted force,

$$F_t = \frac{2M_t}{D} \qquad (3)$$

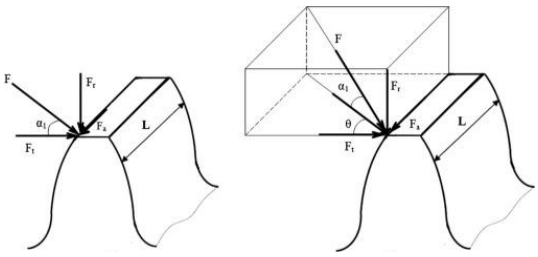

Figure 5.Forces acting on spurl gear

In the design of a gear for strength, the pitch diameter is either known or unknown. If the pitch diameter is known, the following from of the Lewis Equation may be used [6].

$$\frac{1}{m^2 y} = \frac{Sk\pi^2}{F_t} \quad (4)$$

The allowable tooth stress for gear tooth design depends upon the selected material and pitch line velocity. For spur gears,

Allowable $S = S_o \left(\frac{3}{3+v} \right)$ for v<10 m/s (5)

$$S = S_o \left(\frac{6}{6+v} \right) \text{ for v is 10 to 20 m/s} \quad (6)$$

$$S = S_o \left(\frac{5.6}{5.6+\sqrt{v}} \right) \text{ for v>20 m/s} \quad (7)$$

The dynamic load F_d as generally used for average mass condition approximates a more detailed dynamic analysis, as proposed by Buckingham. In SI units, Buckingham's Equation is

$$F_d = \frac{21v(bC + F_t)}{21v + \sqrt{bC + F_t}} + F_t \quad (8)$$

where, F_d = dynamic load, N
v = pitch line velocity, m/s
b = face width, m
F_t = transmitted forced, N
C = a constant, in N/m

Endurance load, F_o

$$F_o = S_o \times b \times y \times \pi \times m \quad (9)$$

To ensure the durability of a gear pair, the tooth profiles must not have excessive contact stress as determined by the wear load F_w.

Wear load

$$F_w = D_p b K Q \quad (10)$$

Where, D_p = pitch diameter of smaller gear, m
b = face width of gear, m
K = stress factor for fatigue, N/m^2

$$Q = \frac{2N_g}{(N_p + N_g)} \quad (11)$$

where, N_g = number of teeth on gear
N_p = number of teeth on pinion

Stress factor for fatigue, K

$$K = \frac{S_{es}^2 \sin\phi \left[\frac{1}{E_p} + \frac{1}{E_g} \right]}{1.4} \quad (12)$$

where, S_{es} = surface endurance limit of gear pair, N/m^2
E_p = modules of elasticity of the pinion material,
E_g = modulus of elasticity of the gear material,
ϕ = pressure angle, degree

The surface endurance limit may be estimated from

S_{es} = (2.75(BHN) -70) MN/m^2 (13)

4.2 For Helical Gear

The allowable stress may be taken as approximately equal to the endurance limit of the material in released loading, corrected for stress concentration effects and multiplied by a velocity factor[5].

Allowable stress,

$$S_{all} = S_o \left[\frac{5.6}{5.6 + \sqrt{V}} \right] \quad (14)$$

In the design, check for strength, the pitch diameter is either known or unknown. If the pitch diameter is known, the following form of the Lewis' equation may be used:

$$\frac{1}{m^2 y} = \frac{S_o k\pi^2 \cos\psi}{F_t} \left(\frac{5.6}{5.6 + \sqrt{V}} \right) \quad (15)$$

where, k= 6
m= module in the plane of rotation, mm
y=the form factor (on the virtual number of teeth)
F_t= tangential force, N
V= pitch line velocity, m/s

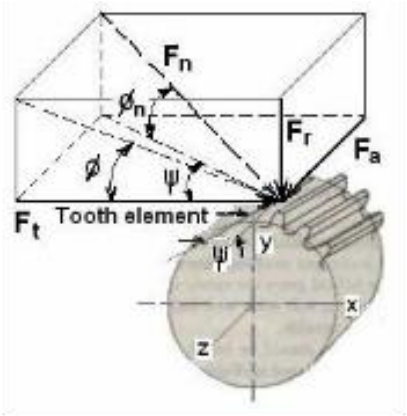

Figure 6.Forces acting on helical gear

The limiting endurance beam strength load, F_0, is based on the Lewis' equation without a velocity factor

$$F_o = S_o b y \pi m \cos\psi \quad (16)$$

where, F_o = the endurance load, N
ψ = helix angle
S_o = the endurance stress, N/m

The limiting wear load, F_w ,for helical gears be determined by the Buckingham equation for wear,

$$F_w = \frac{D_p b K Q}{\cos^2\psi} \quad (17)$$

The dynamic load, F_d , for helical gears is the sum of the transmitted load and an incremental load due to dynamic effect:

$$F_d = F_t + \frac{21V(bC\cos^2\psi + F_t)\cos\psi}{21V + \sqrt{bC\cos^2\psi + F_t}} \qquad (18)$$

TABLE I. Material properties of AISI 5160 OQT 400 and AISI 4340 OQT 400

Material (AISI Number)	Condition	Tensile strength	Yield Strength	Ductility	Brinell Hardness (HB)	Modulus of elasticity	Poissons ratio
		MN/m²	MN/m²			GPa	
4340	OQT 400	1950	1570	11	555	207	0.3
5160	OQT 400	2220	1790	4	627	207	0.3

The input data of spur and helical gears for design calculations are shown in Table II.

TABLE II. In put data for design calculation

Type of gear	Spur gear	helical gear
Maximum power	7.46kW	7.46kW
Pressure angle	20° full depth	20° full depth
Helix angle, ψ	-	35°
Ultimate Strength, S_u	2220 MPa	1950 MPa
Yield Strength, S_y	1790 MPa	1570 MPa
BHN	660	555

5. RESULTS AND DISCUSSION

Gear design is based on known diameter case. AISI 5160 OQT 400 is used in calculating the design for spur gear and AISI 4340 OQT 400 is used for the helical gear. In this machine engine and gear box are connected by V-belt drive. In dynamic force calculation precision cut is used in both gears. In design calculation, strength check and also dynamic check are considered. According to the result dynamic load are less than endurance load and wear load, so design is satisfied for both gear. And then load condition of helical gear is less than spur gear.

TABLE III. RESULT TABLE FOR SPUR AND HELICAL GEAR

	A	B	D	G	F	J	H	K	L	M	M	N
Dp	48.0	64.0	36.0	76.0	68.0	76.0	49.0	175.0	76.0	160.0	160.0	160.0
Tooth, n	24.0	32.0	18.0	38.0	34.0	38.0	16.0	59.0	19.0	40.0	40.0	40.0
rpm	792.0	594.0	594.0	281.4	281.4	251.8	251.8	68.3	68.3	33.0	33.0	33.0
m	2.0	2.0	2.0	2.0	2.0	2.0	3.0	3.0	4.0	4.0	4.0	4.0
b	20.0		25.0		27.0		42.0		43.0		32.0	
Fd (spur)	6117.3		8670.9		9316.5		13315.7		28494.7		27993.8	
Fd (helical)	5480.6		8201.6		8850.3		12992.7		28277.7		27993.8	
Fo (spur)	10787.0		12011.4		11826.3		16912.8		42385.4		36601.3	
Fo (helical)	8909.4		11397.2		9321.4		17238.7		36725.0		28409.2	
Fw (spur)	9855.3		8777.4		10316.1		13567.4		28617.2		34493.5	
Fw (helical)	7085.5		8213.7		8938.5		13166.4		28471.6		30999.0	

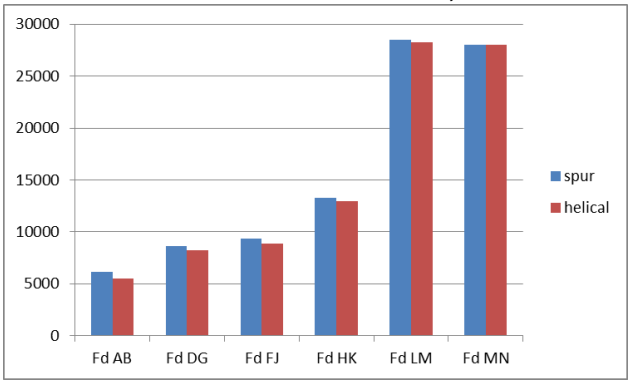

Figure 7. Comparative of dynamic load

Fig. 7 illustrates the amount of dynamic load for the two types of gears. The dynamic loads improve moderately from F_dAB to F_dHK. After then, the loads climb sharply to F_dJM and F_dMN which have the amount of 28494.7 MPa and 28277.7 MPa respectively. Finally, these fall slowly about 27999.8 MPa.

Fig. 8 shows the variation of endurance load for the spur and helical gears. The endurance loads increase slightly at F_OAB and F_oDG but decline slowly at F_oFJ. Then these loads rise gradually. Both of the gears pay the highest endurance loads of 42385.4 MPa and 36725.0 MPa at F_DLM. Then the endurance loads go down considerably at F_DMN.

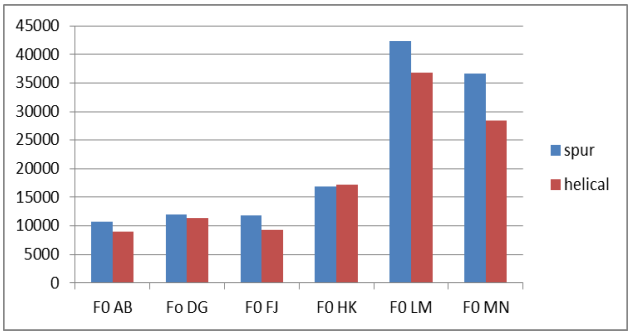

Figure 8.Comparative of endurance load

Fig. 9 indicates the wear load acting on the spur and helical gears. At the beginning of the chart the wear loads are 9855.3 MPa and 7085.5 MPa at F_WAB. Although the wear load for the spur gear decreases slowly at F_WDG, it increases slightly for the helical gear. Then the loads rise steadily from F_WFJ to F_WHK. During the F_WHK and F_WLM, the amount of wear loads climb steeply and then continuous increase significantly to F_WMN.

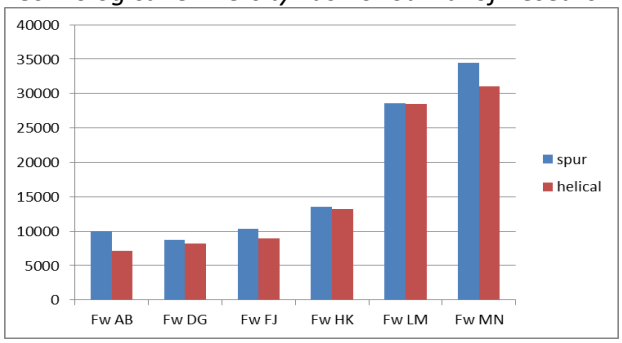

Figure 9.Comparative of wear load

6. CONCLUSION

The design calculation does not change the dimensions of the gear box made of the original spur gear without changing the original velocity ratio. But the original spur gear is made with AIAI 5160 OQT 400 and helical gear is calculated with AISI 4340 OQT 400.The result obtained from the dynamic load in the design satisfied condition show that the endurance load, wear load and dynamic load of the helical gear are less than the spur gear. In term of material hardness, the helical gear is also low. In a helical gear train, the teeth engage a little at a time rather than the entire face at once. This causes less noisy power transfer in case of helical gears. For same tooth size (module) and equivalent width, helical gears can handle more load than spur gears because the helical gear tooth is effectively larger since it is diagonally positioned. The helical gear is smoother to drive than the spur gear, so it is recommended that to use a helical gear made with AISI 4340 OQT 400.

ACKNOWLEDGMENT

The authors would like to thank the Technological University (Lashio), Shan State, Myanmar for hosting this research. The authors would like to express their thanks to Department of Mechanical Engineering, Technological University (Meiktila), for the supporting to develop this paper.

REFERENCES

[14] https://clr.es/blog/en/spur-gears-helical-gears/

[15] Aby Cherian, Jessen .S. Punnan: A Review on Power Tiller Attachments, Scholar, Department of Mechanical Engineering, Amal Jyothi College of engineering, Koovapalli, Kanjirapally, Kottayam, Kerala, India, (2016)

[16] Robert L. Mott, P.E: Machine Elements in Mechanical Design, Fourth Edition, University of Dayton, (2004)

[17] Kubota, 8hp to 14hp Farm Walking Tractor Cultivator Sketch Image. February 2017, http://www.professional-generator.com.

[18] Kubota, 8hp to 14hp Farm Walking Tractor Cultivator Sketch Image. February 2017, http://www.professional-generator.com.

[19] R.S. Khurmi, J.K. Gupta: *Design of Machine Elements*, Eurasia Publishing House (PVT.) Ltd., Ram Nagar, New Delihi-110 055, (2005)

[20] http://www.difference.minaprem.com/solid/difference-between-spur-gear-and-helical-gear/